ZEPHYR - Poloidal Field System

U. Seidel

IPP 1/201 April 1982

Reprint of ZEPHYR-Report No. 13 of May 1980.

MAX-PLANCK-INSTITUT FÜR PLASMAPHYSIK

8046 GARCHING BEI MÜNCHEN

MAX-PLANCK-INSTITUT FÜR PLASMAPHYSIK

GARCHING BEI MÜNCHEN

ZEPHYR - Poloidal Field System

U. Seidel

IPP 1/201 April 1982

Reprint of ZEPHYR-Report No. 13 of May 1980.

Die nachstehende Arbeit wurde im Rahmen des Vertrages zwischen dem Max-Planck-Institut für Plasmaphysik und der Europäischen Atomgemeinschaft über die Zusammenarbeit auf dem Gebiete der Plasmaphysik durchgeführt.

IPP 1/201

U. Seidel

ZEPHYR - Poloidal Field System

April 1982 (in English)

Abstract

The basics of the poloidal field system of the ZEPHYR experiment are considered. From the physical data the requirements for the poloidal field are derived. Hence an appropriate coil configuration consisting of coil locations and corresponding currents is obtained. A suitable electrical circuit feeding the coils is described. A preliminary assessment of the dynamic control of the poloidal field system is given.

Content

1. Introduction

The PF-system for ZEPHYR serves the same fundamental purpose as any other PF-system in Tokamaks.

In detail it has

- To set up and to maintain the plasma current
- To control the plasma position

and

- To shape the plasma cross section

Besides of these functions the PF-system is in the special case of ZEPHYR also assigned

- To heat up the plasma to the ignition point by a fast adiabatic compression

and

- To control the thermal equilibrium of the ignited plasma by adiabatic compression and decompression.

In a more general sense the PF-system can be considered as one possibility (besides the auxiliary heating, gas puffing, ripple control and divertor operation) to control the plasma-parameter and their evolution during the experimental operation.

There are three free poloidal field parameters available to control the plasma

- The poloidal magnetic flux (Φ_{pol}) (governing the plasma flux balance)

- The poloidal field strength $\left(B_{pol} \sim \frac{d\phi_{pol}}{dR} \right)$
  (determining the MHD equilibrium)
- The decay index of the poloidal field $n = \frac{R}{B}\frac{dB}{dR} \sim \frac{d^2\phi_{pol}}{dR^2}$
  (shapening the plasma cross section)

These PF-quantities are functions of virtually all free global plasma variables:

- R_p: major plasma radius
  (follows from the MHD equilibrium)
- a : minor plasma radius
  (determined by the limiter aperture and the toroidal flux balance)
- ε : ellipticity of the plasma cross section
  (function of the vertical field decay index)
- J_p: toroidal plasma volume current
  (determined by the poloidal flux balance inside of the plasma-inclusive diffusion and the plasma energy balance)
- J_{psk}: toroidal plasma skin current
  (following from the poloidal flux balance outside of the plasma-inclusive diffusion)
- ℓ_i : inner plasma inductivity
  (describing the current profile as a result of the pressure balance inside of the plasma)
- n, T $\Big\}$ β_p density and temperature are functions of the plasma energy balance and transport processes (inclusive outer sources of heating and neutral gas)

Thus the knowledge of only those 3 plasma parameters directly controllable by the PF-system is insufficient for a evaluating of the PF-parameters. Rather it is necessary to know all the global plasma variables mentioned above. As indicated these plasma variables are determined by the action of a highly nonlinear and time dependent system consisting of

- the poloidal field system
- the outer sources of heating and neutral gas and
- the plasma

Unfortunately a plasma model of such a generality does not exist. This problem has been solved in the past by a physical-technical optimization process [1]. It has lead to the definition of the experiment and has provided a comprehensive set of plasma parameters describing the desired plasma state at different time points of the experiment. They consist in a prescription of the major plasma radius and of the plasma current. Further are given the presumable temperatures and values of β_p. This information is used in this following report for a preliminary estimation of the PF quantities, there basic time evolution and for a proposition to realize them.

But it should be pointed at some insufficiencies of this kind of physical model consisting only of informations about steady state values of the plasma variables at different times. The model does not provide any detailed information about the dynamic properties of the system and therefore also about the behaviour of the plasma

variables during the transition between plasma states. Furthermore, it may not even be possible to transpose the assumed plasma variables between two different states.

The demand for a comprehensive and selfconsistent plasma model will be encountered again when dealing with the problems related to the final control of the plasma-PF-system.

A further problem arises due to the eddy currents in the vacuum vessel and in the structure, which will affect strongly the dynamical properties of the total system. This problem is under consideration elsewhere.

2. Poloidal Field Requirements

2.1 Basic Data

The requirements of the PF-system are essentially determined by the evolution of the major plasma radius and the plasma current. This evolution is shown schematically in Fig.1. Also plotted are the evolution of the plasma temperature, minor radius and β_p, thus constituting the above mentioned sets of plasma parameters which are needed to evaluate the PF magnitudes. They are derived from the data of the ignited final plasma.

The minor radius a follows from the conservation of the toroidal flux: $\frac{R_p}{a^2}$ is constant.

The plasma current and β_p before the compression were obtained from a flux conserving, free boundary MHD equilibrium calculation [2]. The temperature of the uncompressed plasma results from the simple adiabatic scaling $\left(T \sim \left(\frac{R}{R_o}\right)^{-4/3}\right)$. In the other experimental phases β_p scales as $\frac{T}{J_p^2}$.

Lacking of a sufficiently reliable plasma model for the build up phase PLT-results [3] are scaled to the parameter of ZEPHYR. Thus for the temperature after the current build up was found:

$$T_{eo} \approx 0.7 \left(\frac{J_p}{a}\right)^{4/5} \quad (Z_{eff} \approx 1.1) \text{ [MA, m, keV]} \qquad (1)$$

This result is used for the evaluation of the ohmic flux needed during the buildup phase; as the resistive volt-seconds of this

phase represents only a small part of the total required flux, the results are not very dependent on the assumption of (1).

There are some restrictions concerning the time scales of the buildup phase imposed by the limited available electrical power and the diffusion behaviour of the plasma as well. The total time for the current buildup phase $\tau_{rise} \approx 0.5$ sec. was chosen to keep constant the ratio of this current rise time to a classical skin time (scaling as $\tau_{sk} \sim \kappa a^2 \sim a^{0.8} \cdot J_p^{1.2}$) of ZEPHYR and PLT.

In the early phase of the current rise this assumption is doubtful because of the observed anomalous character of the current penetration [4].

For the purpose of this report the plasma is shut down by reversing the buildup phase. This method raises concerns about the MHD stability of the plasma after the decompression. Until a more detailed study of the plasma shut down is carried out the procedure in Fig.1 will be used.

The values of ℓ_i follow from the ansatz for the profiles in the MHD equilibrium calculation [2]. From there was obtained $\ell_i \approx 1.1$ before and $\ell_i \approx 1.0$ after the compression as a consequence of the flux conservation during the compression.

2.2 Poloidal Flux and Field Strength Requirements

In this section the

- flux ϕ_{pol}, the
- field strength B_{pol} and the
- decay index n

of the poloidal field generated by active coils are calculated.

The conditions to be satisfied by these parameters can be expressed in terms of ϕ_{pol}

$$\frac{1}{2\pi R}\frac{d\phi_{pol}}{dR}\Bigg|_{R=R_p} = B_{pol}\Big|_{R=R_p} = B_{eq}(R_p, J_p, \ell_i, \beta_p, a) \qquad (2)$$

equilibrium condition

$$n = \frac{R}{B_{pol}}\frac{dB_{pol}}{dR} \approx -0.8 \cdots 0.0 \text{ for } R_p - a < R < R_p + a \qquad (3)$$

depending on β_p to obtain a circular plasma cross section and

$$\Delta\Phi_{pol} - \Phi_{Jp} - \Phi_{\Omega} = \Phi_{ptot} = 0 \qquad (4)$$

the steady flux balance, where

Φ_{Jp} is the flux generated by the plasma current and

$\Phi_{\Omega} = \int J_p X dt$ is the flux part covering the ohmic losses to set up and maintain the plasma (X is the resistivity of the plasma column)

It will be shown next that equat. (4) is satisfied at the magnetic axis.

From Eq.(4) can be separated the ohmically consumed flux-part Φ_{Ω}, the remaining equation represents the flux balance of an ideally conductive plasma:

$$(\Delta\Phi_{pol} - \Phi_{\Omega}) - \Phi_{Jp} = \Phi_{ptot} \qquad (4a)$$

$$\Delta\phi_{pol\ inductive} - \Phi_{Jp} = \Phi_{ptot}$$

Because of the axial symmetry of the configuration the condition (4)

$$\Phi_{ptot} = \int_{0}^{t} U_{tor}\, dt = 0$$

means also

$$\int E_{tor}\, dt = 0$$

and since this is supposed to be valid at any time

$$E_{tor} = 0$$

This condition is generally not to satisfy all over where

$$\nabla x E_{tor} = -\frac{\partial B_p}{\partial t} + \nabla x (V_{pol} \times B_p) \neq 0$$

(B_p total poloidal fieldstrength).

but can be fulfilled because of $B_p = 0$ at the magnetic axis. Therefore the inductive flux balance (4a) is satisfied at the magnetic axis of the plasma.

In order to separate the different functions of the poloidal field, it is usually split up in 2 independently controllable flux parts, called "ohmic heating flux" and "vertical field flux"

$$\Phi_{pol} = \Phi_{OH} + \Phi_{v} \qquad (5)$$

They are choosen such that

$$B_{OH} \simeq 0$$

$$B_v = B_{eq} \left(\frac{R}{R_p} \right)^n \qquad (5a)$$

in the plasma region: $R_p - a < R < R_p + a$.

Thus it is possible to adjust the equilibrium field and the decay index alone by the vertical field and the flux balance by the OH-field. From (2), (3), (4) and (5) the following defining equations for the poloidal field parameters are obtained:

$$B_v = B_{eq}(R_p, J_p, \ell i, \beta_p, a) \qquad R = Rp \qquad (6a)$$

$$\frac{R}{B_v} \frac{dB_v}{dR} \approx -0.8 \cdots 0.0 \qquad R_p - a < R < R_p + a \qquad (6b)$$

$$\Delta\Phi_{OH} + \Phi_v = \Phi_{Jp} + \Phi_\Omega \qquad R = R_{mag.axis} \qquad (6c)$$

The characteristic PF-quantities are calculated by a free boundary MHD equilibrium calculation [2]. This calculation solves the equilibrium condition (6a) for a certain decay index (6b) given in terms of relative currents flowing at fixed coil positions. The vertical field current distribution that resulted in a circular plasma cross section was found by a iteration procedure.

From the equilibrium calculation the following is obtained:

- The factor by which the relative currents in the vertical field coils are to be multiplied in order to obtain the required vertical field strength.
- A poloidal equilibrium flux configuration

$$\Phi_{eq} = \Phi_{Jp} - \Phi_{v} \tag{7a}$$

with the OH flux determined from

$$\Delta\Phi_{OH} = \Phi_{eq} + \Phi_{\Omega} \quad \text{for} \quad R = R_{magn.axis} \tag{7b}$$

and in the case of the compression

- the plasma volume current (from the flux conservation)
- the change in the OH-field magnitude which is required to avoid skin currents at the plasma surface.

The radial distribution of Φ_{Jp}, Φ_{v} and Φ_{eq} is shown in Fig. 2 at several times during the pulse. Fig. 3 shows the Φ_{eq} - pattern for the uncompressed and the compressed plasma as well.

In order to figure out from (7b) the total OH-flux change $\Delta\Phi_{OH}$ the resistive volt seconds Φ_{Ω} have still to be estimated.

$$\Phi_{\Omega} = \int_{o}^{t} J_p \; X_p \; dt \qquad X_p : \text{plasma resistivity} \tag{8}$$

Assuming the SPITZER resistivity equation (8) becomes

$$\Phi_{\Omega} = 2.65\ 10^{-2}\ \frac{R_p}{a^2}\ f \cdot \int J_p\ T_{eo}^{3/2}\ dt \tag{9}$$

where R_p and a in m, J_p in MA, T_{eo} in keV and Φ_{Ω} in vs.

f depends on the temperature and current profiles and on Z_{eff} (see appendix A)

For the build up phase the plasma current was assumed as

$$J_p = J_{po}\ (1 - e^{-t/\tau})$$

The plasma temperature follows from this by the integration of a simple energy balance equation

$$\frac{dE}{dt} = J_p^2 - \frac{E}{\tau_E}$$

where τ_E is the energy confinement time; it is assumed $\tau_E \sim n \cdot a^2$. During the other experimental phases linear changes for T_{eo} and J_p are assumed.

Thus for the build up phase

$$\Phi_\Omega \approx 1.0 \text{ Vs } (f \approx 8, Z_{eff} \approx 1)$$

This value includes a flux portion of 0.4 Vs needed to establish the initial plasma. This portion is scaled from PLT results [4] assuming a R_p-proportional scaling.

For the auxiliary heating phase

$$\Phi_\Omega \approx 0.5 \text{ Vs } (f = 13)$$

and for the flat top phase:

$$\Phi_\Omega \approx 1.0 \text{ Vs } (f = 20)$$

The behaviour of $\Delta\Phi_{OH}$ and Φ_v during the experimental lapse is shown in Fig. 4.

3. Realization

3.1 Poloidal Field Coil Configuration

According to the splitting of the total active poloidal flux in 2 parts Φ_{OH} and ϕ_v there are 2 independent coil systems provided to generate them:

- the OH-coil system and
- the vertical coil system.

Each consist of a set of coils located symmetrically above and below the midplane (z = 0) of the experiment. The location and relative magnitudes of the currents carried by these coils are choosen so that the conditions for the respective field strength (eq.5a) are satisfied.

The characteristics of the vertical field system are presented in Fig. 6 (and table II).

The corresponding information about the OH-coil system is given in Fig. 5 and Table I. The main feature of its design is the generation of the total flux in the inner aperture of the experiment in order to satisfy the condition $B_{OH} = 0$ throughout the entire plasma region. This creates a crucial situation concerning the inner coils of the system forming the so called central transformer (coil pairs - upper and lower - OHIa...h in Fig. 6). The relation between the allowed heating and stresses in the central transformer and its outer radius on the one side and the required plasma current and experimental time on the other side constitute one of the basic

design condition for the geometry of the entire experiment. A tradeoff between these parameters is given in appendix B. A more detailed stress analysis of the total PF coil system exceeding the estimation given in appendix B is carried out elsewhere [5].

3.2. Poloidal Field Power Requirements

The knowledge of the PF coil geometry and the coil currents allows an estimation of the required electrical power and energy.

Fig. 7 shows a schematic diagram of the dissipated powers, the dissipated energies and the temperature rises of the OH-and vertical field coils. The heating process was assumed as adiabatic and starting at the temperature of liquid nitrogen. The coils are made of copper some of them with steel as reinforcement (see also appendix B).

It should be pointed out that the diagrams for energies and ohmic powers in Fig. 7 and in the following figures are schematic, and only the indicated points have been calculated. Due to the uncertain plasma scenario there is no point in drawing the fine details of this waveform.

The peak electrical power and total energy requirements are determined by the inductive properties of the PF system.

Fig. 8 shows a diagram of the inductive matrix and the magnetic energies in the vertical field and OH system, Fig. 9 shows schematically the corresponding powers. These results do not include the effects caused by the reaction of the plasma loop. The error introduced by leaving out the plasma reaction is maximal during the buildup phase and amounts there roughly + 20%. An improved calculation that takes into account the plasma reaction is right now under

consideration.

The special techniques used to generate the high powers for the initiation phase and the compression violate the assumption of linear changing currents (see chapter D). In Fig. 9 the peak powers during these phases are therefore not relevant.

4. Power Supply

4.1. Introduction

In this chapter a power supply circuit which provides the required electrical energy and power for the PF coils is discussed.

The main function of the circuit is to generate the extremely high power levels required during the initiation and the compression phases.

The power for the initiation phase is supplied essentially in the same way as most tokamaks whereas the task to generate the power for the adiabatic compression presents a different problem. The only sensible way of providing this power in the required time scale is through an inductive storage. Three different kinds of circuits were closely investigated and compared in Appendix C. Two of these circuits use inductive storages. The purpose of this investigation is to confirm the superiority and feasibility of solutions with inductive storages; only this alternative is considered in the following proposition for a supply circuit.

Aside from the above requirements the following features are desirable:

- As a matter of course the circuit must provide the possibility of an independent adjustment of the OH and vertical field coil currents.
- There should be an option for a symmetrical set up of the circuit for an easier domination of the voltage appearing in it.

- During the initiation phase the vertical field coil should be supplied by the OH-coil system. This measure would save a considerable amount of power in the vertical field power source. (This condition however might be dropped if the restrictions imposed by this linkage cannot be justified by the saved amount of installed power.)

4.2. Supply Circuit

4.2.1. Basic Functions

A basic circuit satisfying all the mentioned requirements and conditions is schematically shown in Fig. 10. In this section the operation of this circuit is briefly described.

Beginning with the switch state as indicated in Fig. 10 the following phases are passed.

- Preloading Phase

Br_v and S1 are closed and L_{OH} and L_{ST} are loaded by the respective sources V_{OH} and V_{ST}. After the current through L_{OH} has reached its negative premagnetization amplitude the source voltage V_{OH} is driven to zero. Then S2 is closed and the current J_{OH} (may be supported by a small corresponding voltage V_{OH}) commutates to the breaker (Br_{OH}) branch. The source current vanishes and S1 is opened. V_{OH} is then adjusted to its positive maximum voltage and V_v to a value somewhat larger.

The loading of L_{ST} continues until the current J_{ST} has reached its desired amplitude. V_{ST} will then be decreased to a

value required to cover the ohmic losses of L_{ST}.

- Initiation Phase

S3 is closed and the current J_{OH} is forced into the resistor R_{OH} by interrupting the breaker Br_{OH}. The high voltage appearing across L_{OH} and L_v leads to the gas breakdown establishing the initial plasma. The current through L_v adjusted and delayed by a passive network is increased.

When the decaying voltage U_{OH} equals the source voltage V_{OH}, S1 and S4 are closed. This applied a constant voltage across L_{OH} which drives the current J_{OH} further in the positive direction (see Fig. 10). Since the voltage of the source V_v was adjusted to a somewhat larger value than V_{OH}, it now takes over the current J_v and the current through the diode D1 vanishes. S3 can now be opened totally separating L_v from L_{OH}. In the following both coil systems are independently supplied by their respective sources.

S2 should also be opened in order to separate R_{OH} from the V_{OH} source and to avoid unnecessary energy losses there. Since the remaining current in the breaker branch is small and the voltage is limited by V_{OH} the power envolved in this interruption is more than two orders of magnitude smaller than the power to be handled by the real breaker. Therefore this interruption should not cause any serious problems. The need for this interruption operation represents a disadvantage of this kind of circuit but offers on the other side the possibility of using the OH breaker (which would be unemployed after this phase) also as the breaker in the compression circuit (broken line in Fig. 10 above). The peak power handling

capability of the OH breaker is sufficient to handle the switching required for the compression (even without the capacitive element C_v).

- Ohmic and Neutral Injection Phase

During this phase the state of the switching remains the same as it was at the end of the initiation phase. L_{OH} and L_v are independently supplied by their respective sources in accordance to the current program. The OH circuit remains in this mode for the rest of the experimental cycle.

- Adiabatic Compression

The loading of L_{ST} is finished prior to the compression. The breaker Br_v interrupts the current $J_{Brv} = J_v - J_{ST}$ and J_v increases rapidly (see appendix C). The source voltage V_v is simultaneously increased to the value needed to maintain the enhanced current J_v. After the compression is accomplished, Br_v is closed. The current J_v is controlled during the burning phase alone by V_{OH} again. V_{ST} is then used to establish the appropriate initial current for the decompression in L_{ST}.

- Decompression

Decompression is achieved in the same way as the compression except that the vertical field coils are now regarded as the inductive storage element which delivers its energy to the inductance L_{ST}

- Shut Down Phase

The currents J_v and J_{OH} are reduced to zero by the source V_{OH} and V_v which act now as inverted converter.

The quantitative specification of the different elements of the supply circuit is done in the following section

4.2.2 Specifications

For the following considerations the normalized quantity, u is introduced:

$$u = \frac{U_{OH\ max}}{U_{BD}} \tag{10}$$

Here $U_{OH\ max}$ means the maximum voltage which appears on the OH coil system at the beginning of the initiation phase immediately after the interrupting of the OH breaker.

and U_{BD} the so called "breakdown" voltage induced by $U_{OH\ max}$ along the loop at which the plasma is supposed to be generated.

Then from Fig. 8

$$U_{BD} = U_{OH\ max} \frac{1}{W_{OH}} \cdot \frac{L'_{OH-p}}{L'_{OH}}$$

where W_{OH} represents the total number of turns of all series connected OH coils. The vacuum vessel reaction is neglected (an estimate of the change of U_{BD} by the presence of the vacuum vessel yields a reduction of roughly 25%.)

With (10) and the values for L'_{OH-p} and L'_{OH} from Fig. 8

$$u = \frac{U_{OH\ max}}{U_{BD}} = W_{OH} \cdot \frac{L'_{OH}}{L'_{OH-p}} = 0.72 \cdot W_{OH} \tag{11}$$

and

$$W_{OH} = 1.38\ u \tag{12}$$

From

$$J_{OH\ max} \cdot W_{OH} = \theta_{OH\ max} = 36.12\ MA \quad \text{(see Fig. 5)}$$

the maximum turn current $J_{OH\ max}$ in the OH-system is given by

$$J_{OH\ max} = \frac{1}{u} \cdot 26.2\ MA \tag{13}$$

The corresponding relations for the vertical field are obtained by considering the linkage between both field-systems during the initiation phase. The following changes must occur simultaneously in the coil excitments and in the plasma current (Fig. 4,5,6)

$$\Delta J_p = 1.3\ MA$$

$$\Delta\theta_{OH} = 0.85 \cdot 36{,}12\ MA = 30.7\ MA$$

$$\Delta\theta_v = 0.2 \cdot 5{,}95\ MA = 1.2\ MA$$

The relation between the turns in the both field systems ($U_{OH} = U_v$) is given by

$$w = \frac{W_{OH}}{W_v} = \frac{\frac{\Delta\theta_{OH}}{\Delta J_p} L'_{OH-V} + \frac{\Delta\theta_v}{\Delta J_p} L'_v - L'_{v-p}}{\frac{\Delta\theta_{OH}}{\Theta J_p} L'_{OH} + \frac{\Delta\theta_v}{\Delta J_p} L'_{OH-v} - L'_{OH-p}} \tag{14}$$

$$w = \frac{W_{OH}}{W_v} = 2.16$$

Taking $\Delta\theta_v = 1.5$ MA in order to assure some margins for a final control, then

$$w = \frac{W_{OH}}{W_v} = 2.5 \tag{15}$$

and

$$W_v = 0.55\ u \tag{16}$$

and finally for the maximum turn current $J_{v\ max}$ in the vertical field coils:

$$\frac{\theta_{v\ max}}{W_v} = J_{v\ max} = \frac{1}{u} \cdot 1.6\ MA \tag{17}$$

Using these normalizations (12,13,15,16,17) and the power requirements for both field systems shown in Fig 7 and 9 the different circuit elements of Fig. 10 can be specified.

Energy Sources

The specifications of the energy sources are compiled:

- In Fig. 11 for the OH-field source V_{OH} and
- In Fig. 12 for the vertical field source V_v

The storage loading source V_{ST} is shown

- In Fig. 13a for the case of a capacitive transfer and
- In Fig. 13b for the case of a ohmic transfer

Fig. 11 - 13b include details of the required output current and voltage in terms of u (10), the output power and the total amount of energy to be transfered by the sources.

If the vertical field system were not to be excited during the initiation phase by the OH-field system, the value for $U_{max} \cdot J_{max}$ of the vertical field source would roughly increase by a factor greater than 3 and P_{max} by a factor of 2.

As the storage inductance has not yet been designed the specification for the V_{ST} source represent only a rough estimate. The current loading time has still to be calculated by an investigation of a real storage coil design. In the case of the ohmic transfer the maximum power of V_{ST} could be determined by the need of quickly changing the current J_{ST} after the compression in order to be ready for a "emergency" decompression.

The total required power and energy of the entire PF-system are summarized as follows:

$$P_{max\ tot} \approx 360\ MW$$

$$W_{tot} \approx 800\ MJ$$

OH-Breaker (Br_{OH}) and Resistor (R_{OH})

The current to be interrupted is

$$J_{BrOH} = J_{OH\ max} = \frac{26.2}{u}\ MA \qquad \text{(Fig. 11)}$$

the voltage across the breaker immediately after the interruption is given by

$$U_{OH\ max} = u \cdot U_{BD}$$

The nominal breaker power P_{BrOH} is determined by

$$P_{BrOH} = J_{BrOH} \cdot U_{OH\ max} = 26.2 \cdot U_{BD}/kV\ GVA;\ \text{and}$$

if we assume $U_{BD} = 150V$ for the breakdown voltage; then:

$$P_{BrOH} = 3.9\ GVA$$

This requirement can be satisfied by the use of 2 breakers from JET typ connected in series.

The dissipated Energy W_{ROH} in the resistor R_{OH} is essentially equal to the magnetic energy initially stored in the OH field coils.

$$W_{ROH} \approx 70 \text{ MJ}$$

For the resistor R_{OH} itself we find

$$R_{OH} = \frac{U_{OH\ max}}{J_{Br\ OH}} = u^2 \cdot \frac{U_{BD}}{26.2\ MA}$$

with the assumptions

$$U_{BD} = 150 \text{ V}$$

$$U_{OH\ max} = \pm 20 \text{ KV} = 40 \text{ KV}$$

i.e. $u = 267$, then

$$R_{OH} = 0.4\ \Omega$$

Vertical Field Breaker (Br_v) and Transfer element (R_v or C_v)

The specifications for the circuit elements related to the adiabatic compression are derived in Appendix C. From there we get the nominal power P_{Brv} for the breaker Br_v

$P_{Brv} = 1.62$ GVA ohmic transfer

$P_{Brv} = 354$ MVA inductive transfer

dissipated energy W_{Rv} in the ohmic transfer element R_v

$$W_{RV} = 53 \text{ MJ}$$

or respectively the energy storage capability E_c of the capacitive transfer element C_v

$$E_c = 8.4 \text{ MJ}$$

maximum voltage at the vertical field coils during the compression:

$U_{v\ max} = 105\ u\ V$ ohmic transfer

$U_{v\ max} = 71.3\ u\ V$ capacitive transfer

Stored energy in L_{ST}

$E_{Lst} = 144$ MJ ohmic transfer

$E_{Lst} = 77$ MJ capacitive transfer

Diode D1

The maximum current carried by this diode corresponds to the current in the vertical field coils at the end of the initiation phase. Thus we get from Fig. 12

$$J_{D1\ max} = \frac{2.2}{u}\ MA$$

The required reverse voltage is small and amounts to roughly

$$U_{Di} \approx u\ V$$

Switch S2

S2 has to interrupt the current J_{ROH} remaining after the initiation phase in the resistor R_{OH} against the voltage V_{OH}

$$J_{ROH} = \frac{V_{OH}}{R_{OH}} = \frac{10 \cdot u\ V}{u^2\ U_{BD}} \cdot 26.2\ MA$$

$$P_{S2} = V_{OH} \cdot J_{ROH} = 17.5\ MVA \quad (\text{with } U_{BD} = 150\ V)$$

The specifications developed in the preceeding chapters is exclusively related to the normal operation of the supply circuit. An analysis showing the behavior of the circuit in the case of a current disruption or other technical failure has still to be carried out and might reveal the need for some changes including the introduction of additional circuit elements.

Acknowledgement

I want to thank L. Bromberg from MIT, Cambridge and D.B. Albert, M. Blaumoser, K. Lackner, M. Pillsticker and H. Preis from IPP, Garching for helpful discussions.

Appendix A: Ohmic Flux Requirement

The flux consumed due to the plasma finite resistivity was evaluated by using the SPITZER resistivity [6] with

R: major plasma radius

a: minor plasma radius

x: normalized r-coordinate in the direction of the minor plasma radius ($x = \frac{r}{a}$)

J_p: plasma current

κ: specific conductivity

the ohmic flux is given by

$$\Phi_R = \frac{R}{a^2} \int \frac{J_p}{\int_0^1 \kappa(x) x \, dx} \, dt \qquad \text{(A1)}$$

For κ is assumed

$$\frac{1}{\kappa} = \eta_{spz} + \eta_{spl} \cdot C(x) \qquad \text{(A2)}$$

where η_{spz} means the SPITZER resistivity for $Z_{eff} = Z$:

$$\eta_{spz} = \frac{1.54}{\gamma_E} 10^{-8} \cdot Z_{eff} \, (Te/keV)^{-3/2} \; \Omega m$$

γ_E depends on Z_{eff}:

Z_{eff}	1	3	4	16
γ_E	0.582	0.683	0.785	0.923

C(x) represents a correction accounting for deviations from the SPITZER resistivity (e.g. trapped particle correction)

The radial temperature distribution is described by

$$T_e = T_{eo}\, v(x) \tag{A4}$$

with T_{eo}: electron temperature on the axis

Putting (A2), (A3) and (A4) in (A7) the resistive volt seconds are obtained by:

$$\phi_R = 2.65\ 10^{-2}\ \frac{R}{a^2}\ \frac{0.582\ \frac{Z_{eff}}{\gamma E}}{\int_0^1 \frac{v(x)^{3/2}\ X}{1+\frac{\gamma E}{0.582\ Z_{eff}}\ C(x)}\,dx}\ \int J_p \cdot T_{eo}^{-3/2}\ dt \tag{A5}$$

or

$$\phi_R = 2.65\ 10^{-2}\ \frac{R}{a^2} \cdot f \int J_p \cdot T_{eo}^{-3/2}\ dt \tag{A6}$$

where ϕ_R is in V_s, T_{eo} is in keV, J_p in MA and R,a are in m.

f was evaluated for different assumptions of c(x), v(x) on Z_{eff}.

The results are shown in Table A1.

Table A1

$C(x) = 0$	$v(x) = (1 - x^2)^2$	$v(x) = (1 - x^2)$
$Z_{eff} = 1$	f = 8	f = 5
$Z_{eff} = 2$	f = 13.6	f = 8.5
$Z_{eff} = 4$	f = 23.7	f = 14.8

$c(x) = \frac{1}{1 - 1.9\sqrt{x} + x} - 1$ (trapped part. correct.)	$V(x) = (1 - x^2)^2$	$V(x) = (1 - x^2)$
$Z_{eff} = 1$	f = 34.4	f = 25.4
$Z_{eff} = 2$	f = 41.2	f = 29.8
$Z_{eff} = 3$	f = 52.7	f = 37.1

Appendix B Central Transformer

1. Introduction

The working space of a pulsed coil is restricted

- With respect to the generated maximum flux Φ by the allowable stresses or
- With respect to the operation time τ and the generated flux $\Phi(t)$ by the allowable temperature rise in the coil material.

This limitations provide the necessary conditions for the dimensioning of a optimal transformer generating a required flux Φ (t). Because of the large influence of the outer radius of the central transformer coil over the total dimensions of the experiment we will define as optimal and transformer with the smallest possible outer radius.

The means for accomplishing this optimization is the reinforcement of the relatively low strength conductor-material (copper) by a material of high strength but usually poor conductivity (steel).

2. Models

2.1. Material and Stress Distribution

There are three components of the transformer material: The conductor, the reinforcement and the insulator. The filling factors are expressed by the relations of the corresponding cross sectional areas.

$$\left.\begin{aligned} f_c &= \frac{F_c}{F_c + F_r} \\ f_r &= \frac{F_r}{F_c + F_r} \end{aligned}\right\} \qquad f_c + f_r = 1$$

$$f_j = \frac{F_j}{F_c + F_r + F_j} = \frac{F_j}{F_{tot}} \qquad \text{(B1)}$$

$$f_m = \frac{F_c + F_r}{F_{tot}} = 1 - f_j$$

The used indices c, r and j refer to the conductor, the reinforcement and the insulator. The insulator includes the space required for cooling and structure.

The average stress in the conductor and reinforcement composite can be expressed as:

$$\sigma_m = f_r\,\sigma_r + f_c\,\sigma_c = f_r\,(\sigma_r - \sigma_c) + \sigma_c \qquad \text{(B2)}$$

Depending on the absolute stress magnitude the stress distribution between conductor and reinforcement can be described by two simplified models:

In model A the stresses are sufficiently low so that both materials remain in the elastic region. Then

$$\frac{\sigma_r}{\sigma_e} = \frac{E_r}{E_c} \qquad \text{E: Youngs modulus}$$

and from (B2)

$$\sigma_m = \sigma_c \left(f_c + f_r \frac{E_r}{E_c} \right) = \sigma_c \left(1 + f_r \left(\frac{E_r}{E_c} - 1 \right) \right) \qquad \text{(B3)}$$

In the special case of a steel-copper compound $\frac{E_r}{E_c} = \frac{E_{steel}}{E_{copp}} \approx 2$

this means that because of the relatively low elesticity limit of compper ($\sigma_{0.2} \lesssim 250$ MPa) the potential steel strength can not be utilized completely. The validity of this model is generally restricted to low stress levels.

Model B refers specifically to a steel-copper composite. The stresses are large and the copper is deformed plastically. In such a composite after several loadings a final stress appears of $\sim$ 150 MPa in the copper [7]. A corresponding change is observed in the steel stress. In this case the maximum stress is given by:

$$\sigma_{m\,max} = (1-f_c)\,\sigma_{rmax} + f_c\,\sigma_{co} \quad \text{with } \sigma_{co} = \text{const.} \simeq 150 \text{ MPa} \tag{B4}$$

2.2. Heating

Because of the relatively short pulse length the temperature rise in the coils is determined by an adiabatic heating process starting at liquid nitrogen temperature.

The thermal energy increase can be written as:

$$j_c^2\, F_c \rho_c(T) dt = (C_c(T) F_c + C_r(T)\, F_r)\, dt \tag{B5}$$

where jc means the current density, ρ the specific conductor resistivity and C_c and C_r the heating capacities of the conductor and the reinforcement.

It is assumed that the conductor and reinforcement are always at the same temperature and that the current flows only in the conductor. Assuming that

$$c(T) = C_c(T) \simeq C_r(T)$$

then (B5) reduces to

$$\Lambda(T) = fc \int jc^2\, dt = \int \frac{C_c(T)}{\rho_c(T)}\, dT \tag{B6}$$

The integral on the right side in (B6) was evaluated for copper [8] and the resulting $\Lambda(T)$ is shown in Fig. B1. If the allowed peak temperature in the transformer is $\leq 273°$ K, then for copper as conductor material:

$$\int j_c^2 \, dt \leq \frac{1}{f_c} \cdot 750 \left(\frac{KA}{cm^2}\right)^2 \text{ sec} = \frac{1}{f_c} \Lambda_o \qquad \text{(B7)}$$

The <u>total thermal energy</u> in the composite per unit volume of conductor is given by

$$\frac{dW_{th}}{dV_c} = \int jc^2 \, \rho(T) \, dt = \frac{1}{f_c} \int c(T) dT$$

$$\frac{dW_{th}}{dV_c} = \frac{1}{fc} W^*$$

W^* is shown in Fig. B1 as a function of $\Lambda = f_c^2 \int j_c \, dt = \int \frac{c(T)}{\rho(T)} dt$

The corresponding power to be provided by the outer sources to cover the resistive losses is given by

$$\frac{dP_{th}}{dV_c} = j_c^2 \, \rho(T) = \frac{1}{f_c} \frac{d\int c(T)dT}{d\Lambda} \quad \frac{d\Lambda}{dt}$$

and with $\Lambda = f_c \int j_c^2 \, dt$ and (B7)

$$\frac{dP_{th}}{dV_c} = \frac{dW^*}{d\Lambda} \cdot j_c^2 \qquad \text{(B8)}$$

$\frac{dW^*}{d\Lambda}$ can be obtained from Fig. B1. It represents nothing else than $\rho(\Lambda)$.

2.3 Transformer:

The following considerations are restricted to a totally homogeneous transformer such that

$$j_c = \text{const and}$$
$$f_c = \text{const} \tag{B9}$$

It should be pointed out that it is possible to further optimize the transformer by dropping these assumptions. An additional simplification is attained by treating the transformer as a long coil. Therefore the results are sufficient for a parametric study but must be carefully evaluated in a specific case by a more detailed analysis.

The used geometry is indicated in Fig. B2. The average current density $\bar{j}$ is defined by:

$$\bar{j} = \frac{J_{tot}}{F_{tot}}$$

The average current density in the conductor-reinforcement composite is defined by

$$j_m = \frac{J_{tot}}{F_r + F_c} = \bar{j} \cdot \frac{1}{f_m}$$

The current density in the conductor is given by

$$j_c \frac{J_{tot}}{F_c} = \bar{j} \frac{1}{f_m} \cdot \frac{1}{f_c}$$

Furthermore

$$\bar{\sigma} = f_m \, \sigma_m$$

Here σ_m means the average stress in the composite (see B2) and $\bar{\sigma}$ the stress average over the total cross section. The magnetic field strength is given by

$$\begin{aligned} B &= \mu_o \, \bar{j} \, R_o \, (1 - x) \qquad \text{for } s < x < 1 \text{ and} \\ B &= B_{max} = \mu_o \bar{j} \, R_o \, (1 - s) \qquad \text{for } x < s \end{aligned} \tag{B11}$$

(for the definition of x and s see Fig. B2).

Hence the generated magnetic flux Φ is

$$\Phi = \frac{\pi}{3} B_{max} \, R_o^2 \, \frac{1 - s^3}{1 - s}$$

or with (B11)

$$\Phi = \frac{\pi}{3} \mu_o \, \bar{j} \, R_o^3 \, (1 - s^3) \tag{B12}$$

and solved for $\bar{j}$

$$\bar{j} = \frac{\Phi}{R_o^3} \, \frac{0.76 \cdot 10^6}{(1 - s^3)} = \frac{\Phi}{R_o^3} \quad i(s) \tag{B13}$$

where j is in A/m^2, Φ is in V_s and R is in m

i(s) is shown in Fig. B3.

The electro magnetically generated circumferential stress $\bar{\sigma}_g$ can be found with

$$\frac{\bar{\sigma}_g}{R} = P = \bar{j} \times B, \text{ (B11) and (B12)}$$

and is given by

$$\bar{\sigma}_g = \sigma_{gmax}\, 4\, x\, (1 - x)$$

where

$$\sigma_{gmax} = \frac{1}{4} \frac{\Phi^2}{\kappa_o^4} \frac{9}{\pi^2 \mu_o} \frac{1}{(1 - s^3)^2} \tag{B14}$$

However the deflection $\Delta x \sim \sigma_g \cdot x$ caused by the stress distribution (B14) is not self consistent, as in the outer region of the transformer the deflections do not match. Therefore reaction forces appear modifying the original stress distribution in such a way that the resulting strain in the region in question becomes constant ($\Delta x'$ in Fig. B2). Because of $\sigma \sim \frac{\Delta x}{x}$ this leads to the modified stress distribution $\bar{\sigma}'$

$$\bar{\sigma}' = K \cdot \frac{1}{x} \tag{B15}$$

If the transformer design is such that different layers are capable of transfering radial pressure but not tension then the described force adjusting process must be restricted to a region $x > x_o$

At $x = x_o$

$$\bar{\sigma}'\,(x_o) = \bar{\sigma}_g\,(x_o) \tag{B16}$$

and in order to balance the total force

$$\int_{x_o}^{1} \bar{\sigma}' dx = \int_{x_o}^{1} \bar{\sigma}_g\, dx \tag{B17}$$

Carying out this and using (B14) and (B15) for x_o is obtained

$$x_o = 0.482$$

Thus the maximum stress for a transformer with $s < 0.482$ is:

$$\sigma_{max} = \bar{\sigma}_g(x = 0.482) = \frac{\Phi^2}{R_o^4} \frac{9}{\pi^2 \mu_o} \frac{0.25}{(1 - s^3)^2}$$

or

$$\bar{\sigma}_{max} = \frac{\Phi^2}{R_o^4} \frac{0.181}{(1 - s^3)^2} = \frac{\Phi^2}{R_o^4} \cdot r(s) \quad \begin{matrix} \text{for } s < 0.482 \\ \text{at } x = 0.482 \end{matrix} \qquad \text{(B18)}$$

(V_s, m, MPa)

and $\bar{\sigma}' = \bar{\sigma}_{max} \cdot \frac{0.482}{x}$ for $x > 0.482$

In the case of a transformer with $s > 0.482$ the force balance equation (B16) becomes:

$$\int_s^1 \bar{\sigma}' \, dx = \int_s^1 \bar{\sigma}_g \, dx$$

and hence

$$\bar{\sigma}' = \frac{\Phi^2}{R_o^4} \frac{9}{\pi^2 \mu_o} \frac{1 - s^2(3 - 2s)}{6(1 - s^3)^2 \ln\frac{1}{s}} \cdot \frac{1}{x} \qquad \text{(B19)}$$

the maximum stress appears at $x = s$

$$\bar{\sigma}_{max} = \bar{\sigma}'(x = s) = \frac{\Phi^2}{R_o^4} \frac{9}{\pi^2 \mu_o} \frac{1 - s^2(3 - 2s)}{6s(1 - s^3)^2 \ln\frac{1}{s}}$$

or

$$\bar{\sigma}_{max} = \frac{\Phi^2}{R_o^4} \cdot 0.726 \frac{1 - s^2(3-2s)}{6s(1-s^3)^2 \ell n \frac{1}{s}} = \frac{\Phi^2}{R_o^4} r(s) \qquad \text{for } s > 0.482 \text{ at } x = s \qquad \text{(B20)}$$

(Vs, m, MPa)

The function r(s) in (B18) and (B20) is represented in Fig. B3.

The radial stress σ_p is given by

$$\frac{d\sigma_p}{dx} = \frac{\bar{\sigma}' - \bar{\sigma}_g}{x} \qquad \text{(B21)}$$

$\sigma_p \neq 0$ only for $x > x_o$, as for $x < x_o$ the transformer windings separate from each other.

3. Optimization

(B2), (B7), (B13), (B18) and (B20) constitute the basic set of equations needed to optimize the central transformer. s is choosen to be

$$s = 0.3$$

A smaller value of s introduces little gain (see Fig. 3B) but makes manufacturing more difficult.

Thus with s = 0.3, (B2) and (B7) (B18) and (B13) reduce to:

a) $$\bar{\sigma}_{max} = 0.19 \frac{\Phi^2}{R_o^4} \qquad \text{(B22)}$$

b) $$\bar{j} = 0.78 \cdot 10^6 \frac{\Phi}{R_o^3}$$

c) $$\sigma_m = (1 - f_c)\, \sigma_r + fc\, \sigma_c$$

d) $$\int j_c^2 \, dt = \frac{1}{f_c} \cdot \Lambda_o \qquad \left(\Lambda_o = 750\ 10^{14} \left(\frac{A}{m^2}\right)^2 \text{sec for copper}\right)$$

and additional:

$$j_c = \bar{j}\,\frac{1}{f_m} \cdot \frac{1}{f_c} \quad \text{and} \quad \bar{\sigma} = f_m \cdot \sigma_m \quad \text{from B10}$$

Putting in (B22) (a) in (c) and (b) in (d)

a) $$\frac{0.19}{f_m} \cdot \frac{\Phi^2}{R_o^4} = \sigma_R - f_c\,(\sigma_R - \sigma_c) \tag{B23}$$

and

$$\frac{0.61\ 10^{12}}{f_m^2}\,\frac{\int \Phi^2 dt}{R_o^6} = f_c \cdot \Lambda_o$$

$\Phi = \Phi(t)$ can be characterized by two quantities Φ_o and τ.

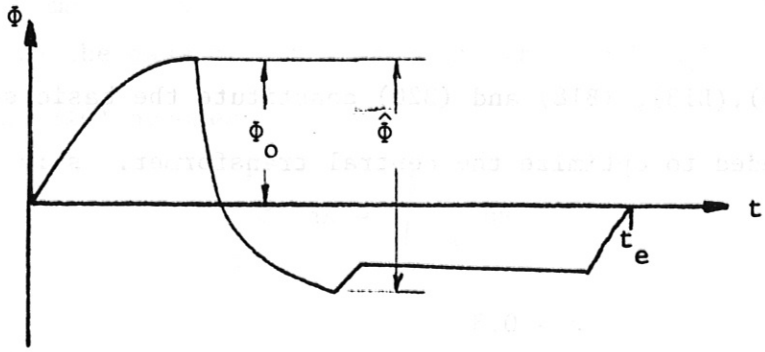

Φ_o represents the absolute maximum value of $\Phi(t)$ and determines the maximum stress. The equivalent pulse length τ is defined by

$$\tau = \frac{\int_o^{t_e} \Phi^2\ dt}{\Phi_o^2} \tag{B24}$$

The flux requirements are on the maximum total flux swing $\hat{\Phi}$ rather than on Φ_o. The requirements on Φ_o and τ are then functionally related by

$$\Phi_o = \Phi_o(\tau) \tag{B25}$$

$\Phi_o(\tau)$ depends on the actual evolution of $\Phi(t)$.

As a further simplification it is assumed that

$$\hat{\Phi} = 2\,\Phi_o$$

The peak stresses at the maximum and minimum values of $\Phi(t)$ are equal. Although not the optimal solution, the results can be easily altered to include the general case of equation (B25).

Using the given definitions for Φ_o and τ equation B23 results in

$$\text{a)}\quad \frac{0.19}{f_m}\frac{\Phi_o^2}{R_o^4} = \sigma_R - f_c\,(\sigma_R - \sigma_c)$$

$$\text{b)}\quad \frac{0.61\ 10^{12}}{fm^2\ \Lambda_o}\frac{\Phi_o^2}{R_o^6}\cdot\tau = f_c \tag{B24}$$

or separated with respect to R_o and f_c to be determined:

$$\text{a)}\quad R_o^6 - R_o^2\,\frac{0.19}{f_m}\frac{\Phi_o^2}{\sigma_R} = \frac{0.61\ 10^{12}}{f_m^2\ \Lambda_o}\left(\frac{\sigma_R - \sigma_c}{\sigma_R}\right)\Phi^2\cdot\tau$$

$$\text{b)}\quad f_c(\sigma_R - \sigma_c) + f_c^{2/3}\ 2.62\ 10^{-9}\ f_m^{1/3}\left(\frac{\Lambda_o\Phi_o}{\tau}\right)^{2/3} = \sigma_R \tag{B25}$$

[m, A, Vs, MPa]

From (B25b) follows the practical important condition for the allowable stress in the conductor that makes a reinforcement dispensable.

With fc = 1 we get for this stress σ_{co}

$$\sigma_{co} \geq 2.62\ 10^{-9}\ f_m^{1/3} \left(\frac{\Lambda_o \Phi_o}{\tau} \right)^{2/3} \qquad \text{(B26)}$$

The radius for such a reinforced transformer is then determined by the allowed temperature rise alone; from (B24b)

$$R_o = \sqrt[6]{\frac{0.61\ 10^{12} \Phi_o^2\ \tau}{f_m^2 \cdot \Lambda_o}} \qquad \text{(B27)}$$

For a steel-copper composite with

$$\sigma_{steel} = \sigma_R = 900 \text{ MPa}$$

$$\sigma_{copper} = \sigma_c = 150 \text{ MPa} \qquad \text{(material model 'B')}$$

$$\Lambda_o = 750\ 10^{14} \left\{ \frac{A}{m^2} \right\}^2 \text{sec}$$

and $$f_m = 0.8$$

a graphic representation of (B25) is shown in Fig. B4.

For a required Φ_o and τ the copper share f_c in the composite and the outer radius R_o of the transformer can be read from Fig. B4.

The requirement for a certain fluxswing $\hat{\Phi}$ rather than for a Φ_o would be represented in this diagram by a curve accordingly to (B25). The optimal solution in this case would then be indicated by the smallest radius touched by this curve.

Summarizing, a solution has been found that makes the best use of the thermal coil limits and leads to a homogeneous temperature rise throughout the entire transformer cross section; however this solution utilizes the strength only at a certain radius. At different

radius the stresses are smaller than the potential strength. It is possible to further decrease the energy losses by making the maximum allowable stresses at a given radius equal to the local stress. This can be done by adjusting the conductor share f_c. However, an additional mechanical loading would appear by the radial temperature gradients.

A similar optimization procedure has been carried out in which both the heating and the mechanical loading limits were used to theirs full extent. A possible flux gain of roughly 20% has been realized in this design as compared with the results presented above. This design requires not only a radial variation of the conductor-reinforcement ratio but also a radial variation of the current density. A detailed presentation of these results is outside the scope of this report.

Appendix C: Compression Circuits

1. Requirements

The engineering problem of realizing the adiabatic compression can be reduced to the need of increasing the current through an inductive circuit element by a factor of 2 in a relatively short time ($t_c \approx 0.15$ sec). The electromagnetical reaction of the currents in the OH-coils and in the plasma can be neglected because the flux change in the vertical field caused by them are very small. (The current in the OH-coils is virtually constant and the effect of the plasma current increase is canceled by a corresponding decrease of the mututal inductance). Different methods to realize the current rise lead to different compression speeds. The condition for the adiabatic compression (fast compared to the energy confinement time) is not satisfied to the same degree for the different circuits. Solutions generating a high initial speed ($\dot{J}_v$) and a lower final speed are prefered.

Fig. C1 indicates the basic requirements. Normalization quantities are also defined in Fig. C1.

2. Realization

Three suitable circuits are described and compared in this section:

Circuit A (inductive storage with ohmic transfer)

This method is proposed for the adiabatic compression in JET [9].

The energy transfer from the inductive storage element to

the vertical field coils is caused by interrupting the current difference $J_{stuc} - J_{vuc}$, forcing this current into the resistor R and thus generating a voltage across L_v. The resulting transient responses of the different quantities are shown in Fig. C2 together with formulas describing the respective amplitudes.

After the compression is accomplished the breaker may remain opened.

Because of the $(1 - e^{-t/\tau})$ character of the current transition, the time needed to cover 90% of the current rise has been arbitrarily stipulated as the compression time.

A characteristic of this circuit is its poor efficiency due to the large energy losses in the resistor.

Circuit B (inductive storage with capacitive transfer) See Fig. C3

This circuit acts in exactly the same way as circuit A except that the resistor is now replaced by a capacitor thus reducing the energy losses. As a result the powers and energies are considerably reduced. The breaker must be closed again after the compression has been accomplished. The resulting transition curve has a $(1 - \cos \omega t)$ behaviour.

Circuit C (capacitive storage) See Fig. C4

This method might be used for the adiabatic compression in TFTR [10].

Here the energy to be transfered into the vertical field coils is stored merely in a capacitor bank. The initial vertical coil current is bypassed from the storage device by a diode. The compression

is started by closing the switch S applying the storage voltage to the vertical field coils and biasing the diode in the reverse direction. The resulting circuit acts like an oscillator circuit transferring the energy from the capacitor to the inductor. A reversing of this process is prevented by the diode acting now as a bypass to the condensor bank again.

Using the numerical values of Fig. C1 for ZEPHYR the characteristics of these circuits are now discussed.

The relation of the inductive storage element to the inductance of the vertical field coils was choosen in the case of circuit A to minimize the stored energy; in the case of circuit B it is choosen as a compromise between the stored energy and the energy storing capability of the capacitor bank (see Fig. C3a). Hence is obtained a comparing representation of the characteristical values and properties of the different circuits in Table CI.

This table illustrates the differences between circuits A and B: The energies and powers in circuit A are much higher than in circuit B. The advantages of circuit B are opposed by the need for the very large but unloaded capacitor bank. The advantages of circuit B may be reduced further if the main OH-breaker is used for the compression. This breaker easily meets the requirements for the circuit A breaker. The suitability of circuit C is questionable because of the very large and preloaded capacitor bank.

The ratings indicated by "decompression" address the capability of the circuits to perform the decompression. Circuit A

and B can be used in exactly the same way for the decompression. In circuit B the plasma can be decompressed immediately after the compression by a simple new interruption; in circuit A the plasma can not be decompressed until some change in the storage coil current is accomplished. This difference might be important with regard to disruption control.

The term "current rise shape" in Table CI relates to the quality of the behaviour of the compression speed resulting in the different circuits.

Table CI

Circuit A (induct. storage & ohmic transfer)	Circuit B (inductive storage & capacitive transfer)	Circuit C Capacitive storage
$\ell = 0.32$	$\ell = 0.5$	
Stored energy:		
$E_{st} = 1.87$ Eve	$E_{st} = $ Eve	$E_{st} = 0.72$ Eve
$= 144$ MJ	$= 77$ MJ	$= 55$ MJ
(inductive)	(inductive)	(capacitive)
Switch Power:		
$P_B = 3.15 \frac{Eve}{tc}$	$P_B = 0.69 \frac{Eve}{tc}$	$P_D = 1.71 \frac{Evc}{tc}$
$= 1.62$ GW	$= 354$ MW	$= 880$ MW
(breaker)	(breaker)	(diode)
Energy in Transfer element:		
$E_R = 0.68$ Evc	$E_c = 0.11$ Evc	
$= 53$ MJ	$= 8.4$ MJ	----------
(ohmic)	(capacitive)	
Decompression:		
(+)	(++)	(-)
Current rise shape:		
(+)	(-)	(+)

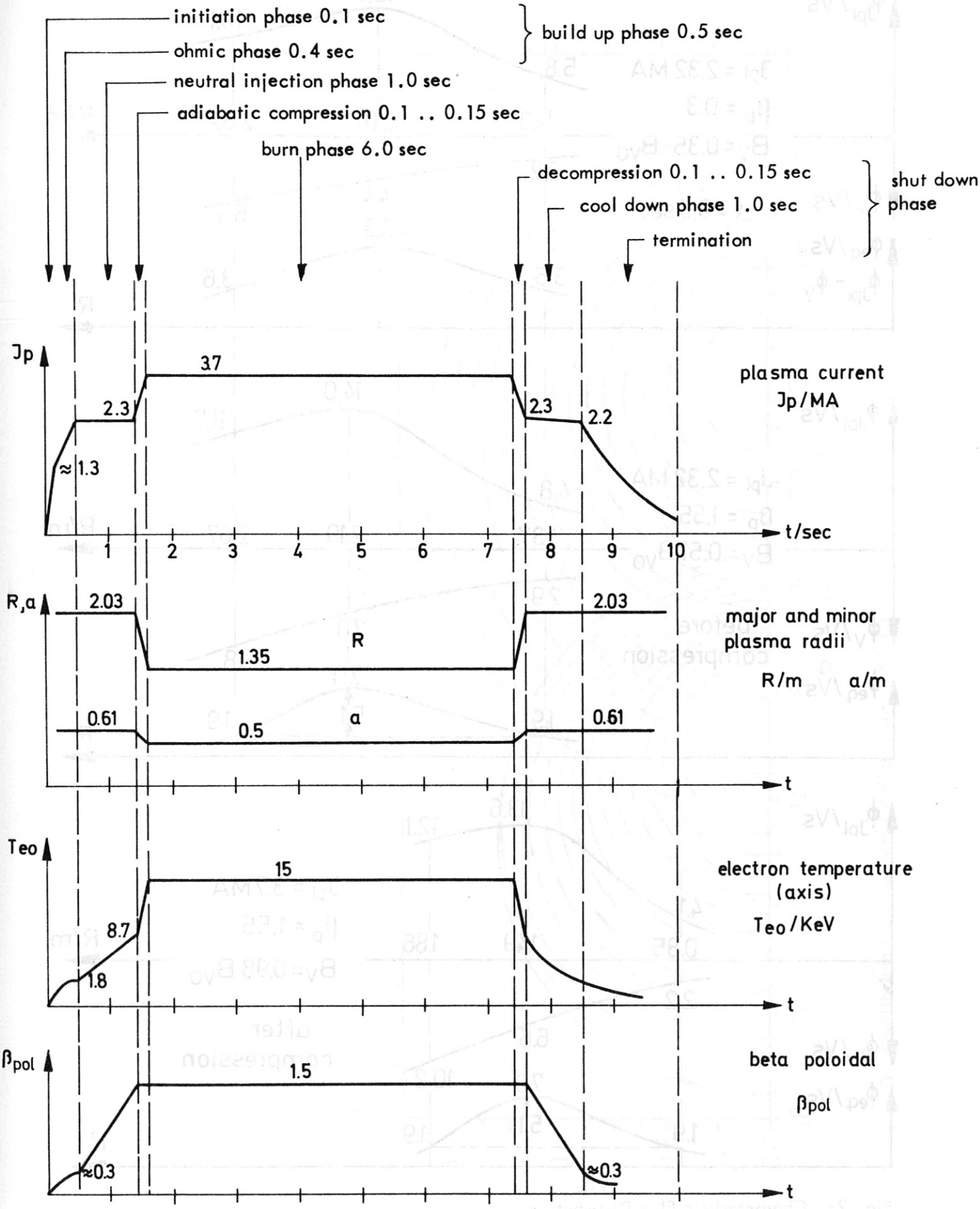

Fig. 1: Basic Data

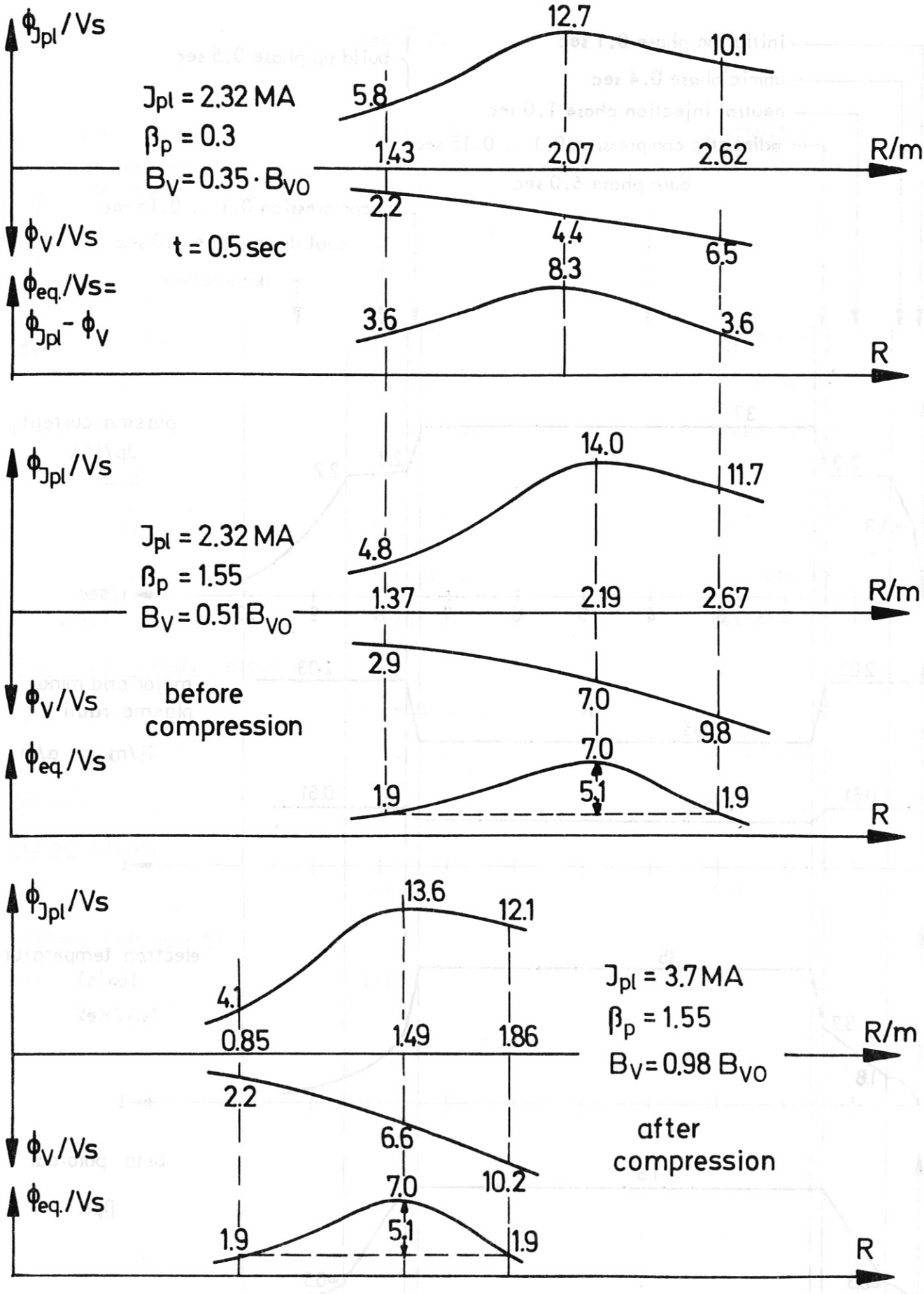

Fig. 2: Characteristic Flux Distribution

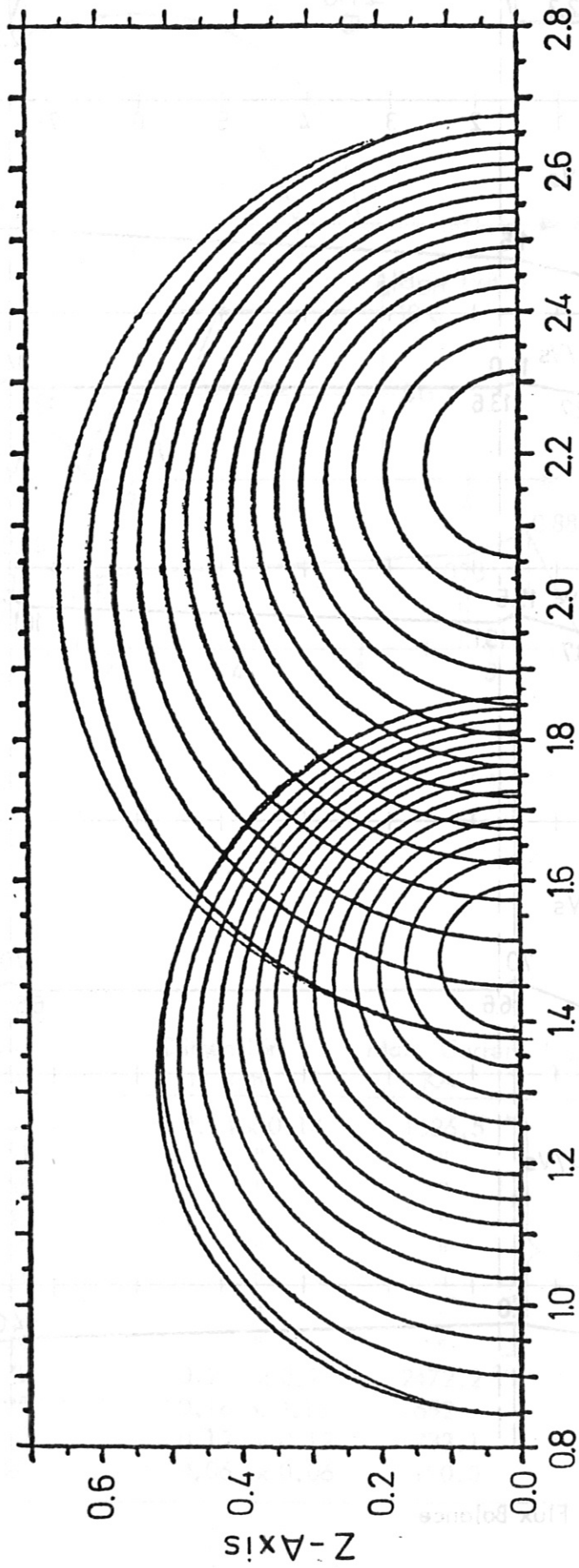

Fig. 3: Equilibrium Flux Surfaces Configuration (PSIGES)

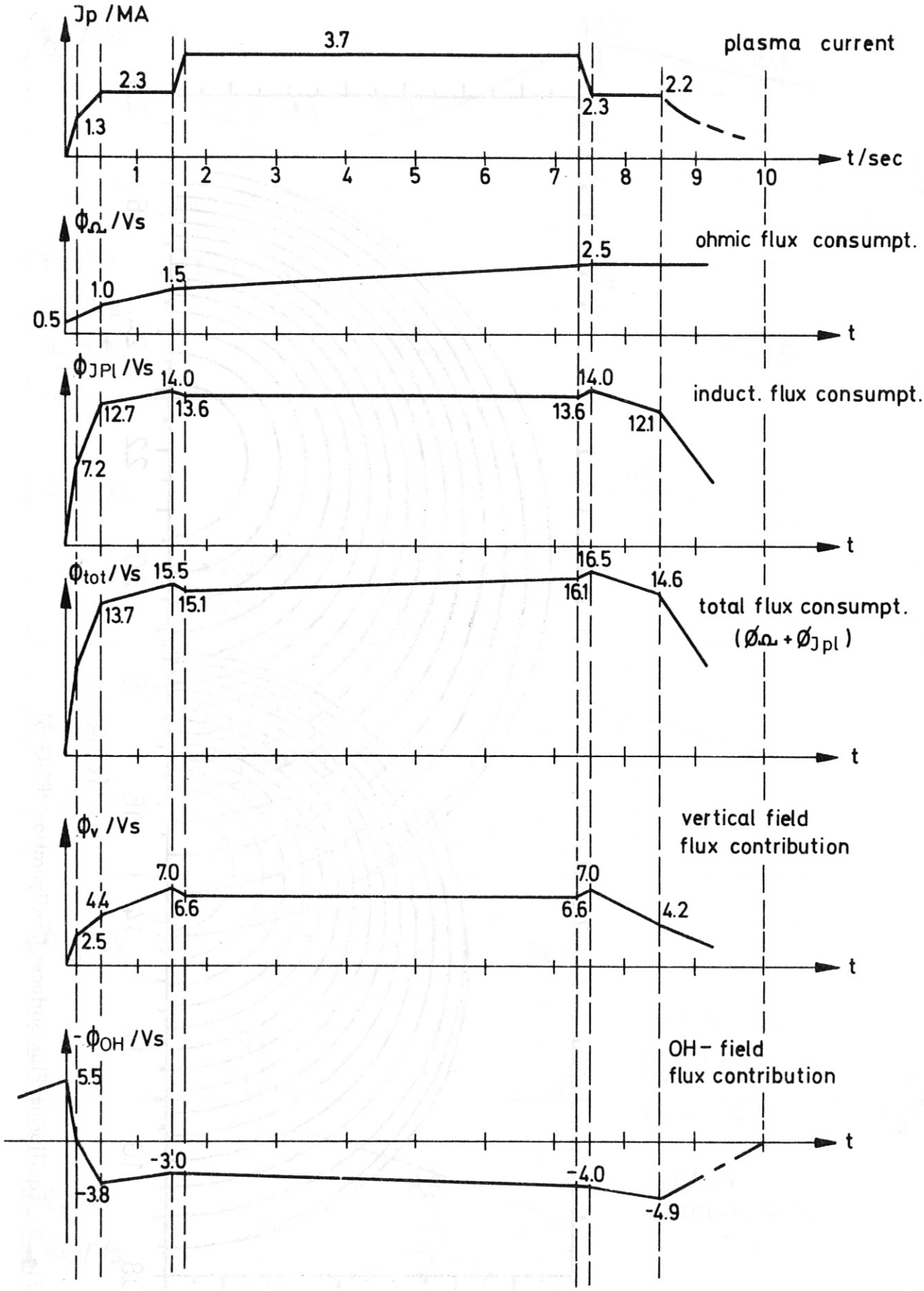

Fig. 4: Flux Balance

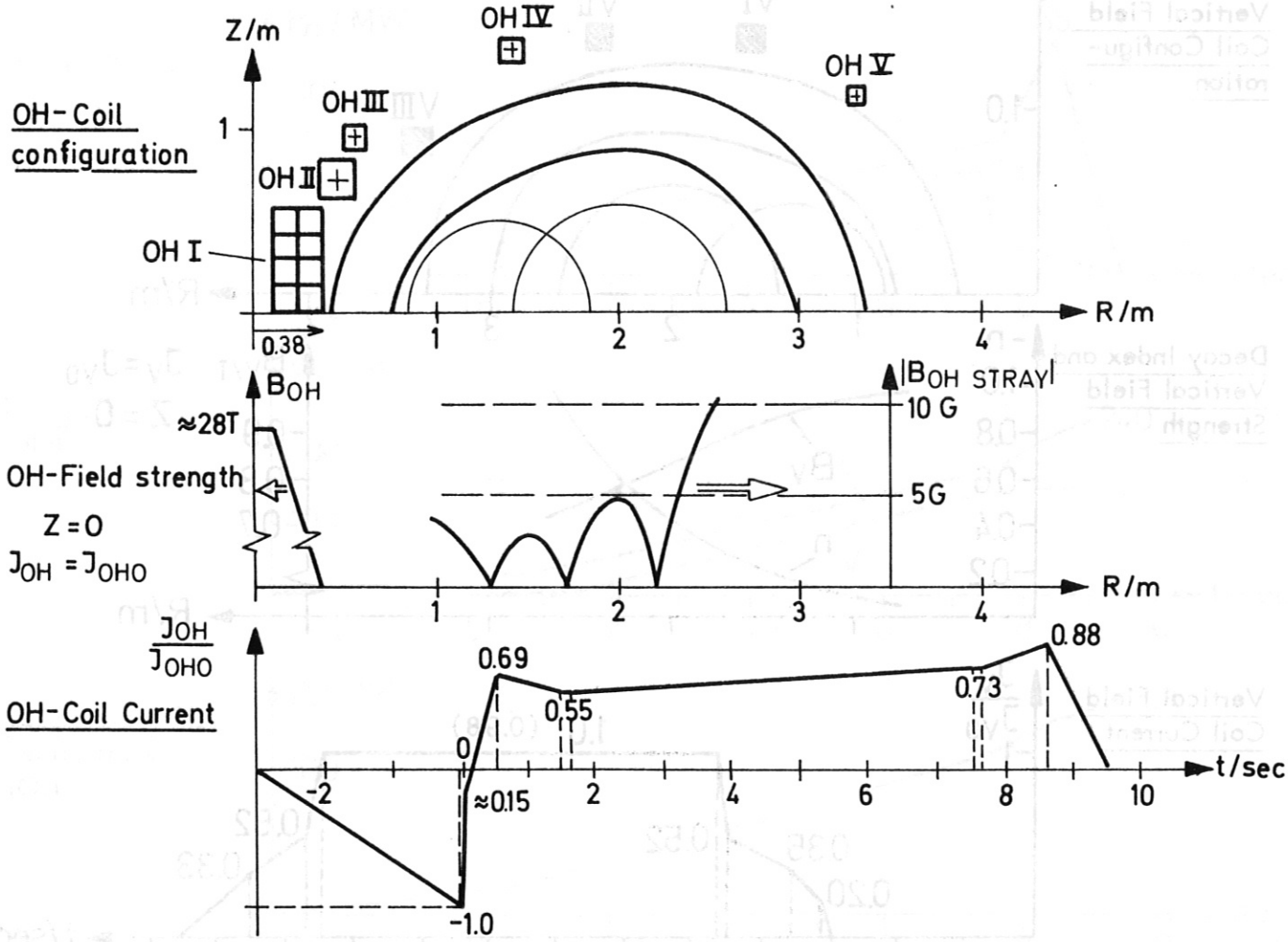

Table I

Coil		Center Location R/m	Center Location Z/m	Dimension m x m	Max. Current J_{OHO} KA	
OH I	a	0.17	0.07	0.14 x 0.14	1626.5	central transformer
	b	"	0.21	"	"	
	c	"	0.35	"	"	
	d	"	0.49	"	"	
	e	0.31	0.07	"	"	
	f	"	0.21	"	"	
	g	"	0.35	"	"	
	h	"	0.49	"	"	
OH II		0.45	0.72	0.2 x 0.2	2472.2	
OH III		0.60	0.95	0.16 x 0.16	1652	
OH IV		1.45	1.40	0.12 x 0.12	733.1	
OH V		3.3	1.20	0.06 x 0.06	190.0	

$J_{OH\,total} = 2 \times \Sigma J_{OHO} = 36.12$ MA

Fig. 5: OH Coil System

Vertical Field Coil Configuration

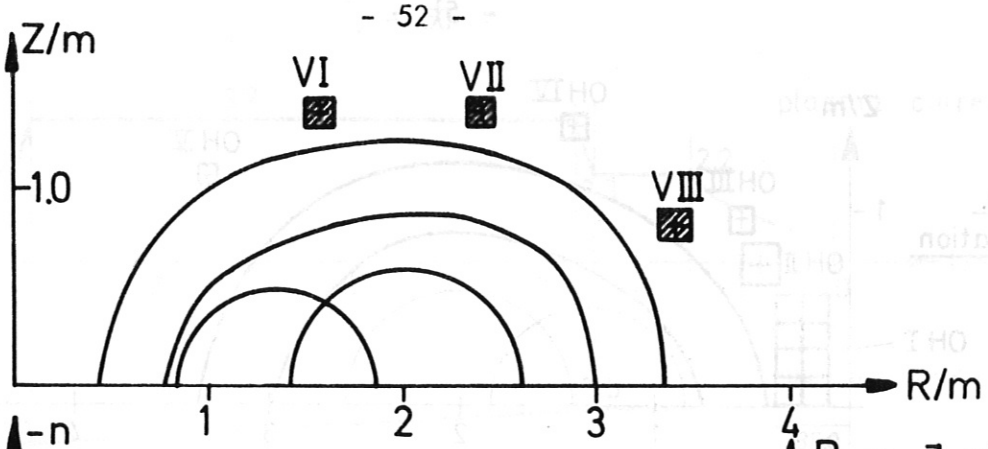

Decay Index and Vertical Field Strength

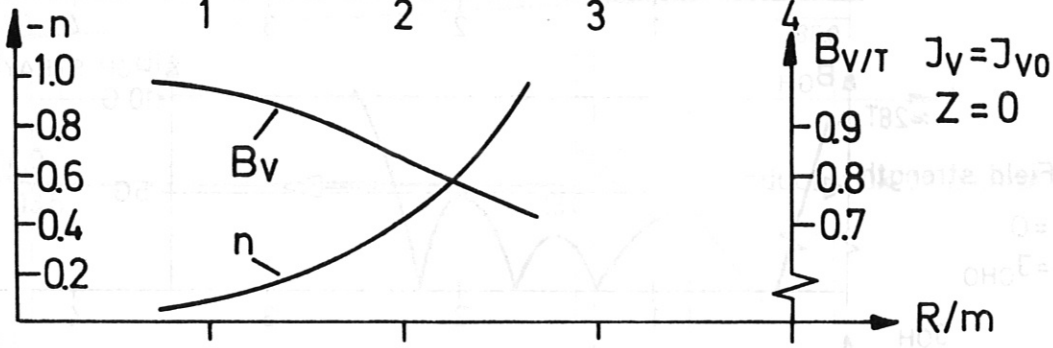

Vertical Field Coil Current

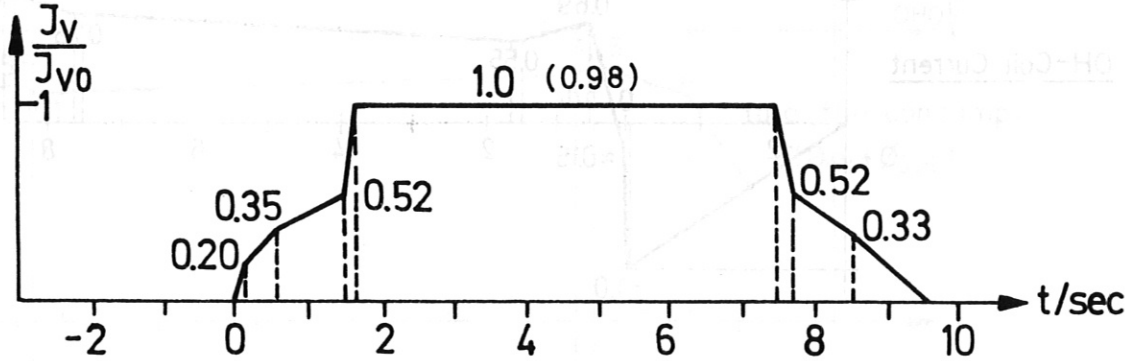

Table II

Coil	Center Location R/m	Z/m	Dimension m x m	Max. Current J_{vo} KA
VI	1.6	1.4	0.1 x 0.1	558
VII	2.4	1.4	0.14 x 0.14	930
VII	3.4	0.8	0.18 x 0.18	1488

$J_{v\,total} = 2 \times \Sigma J_{vo} = 5.95$ MA

Fig. 6: Vertical Field Coil System

Dissip. Power total

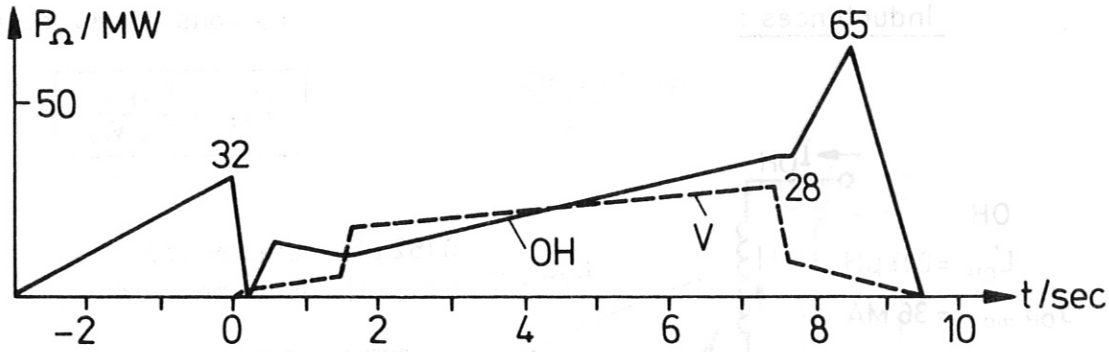

Dissip. Energy total

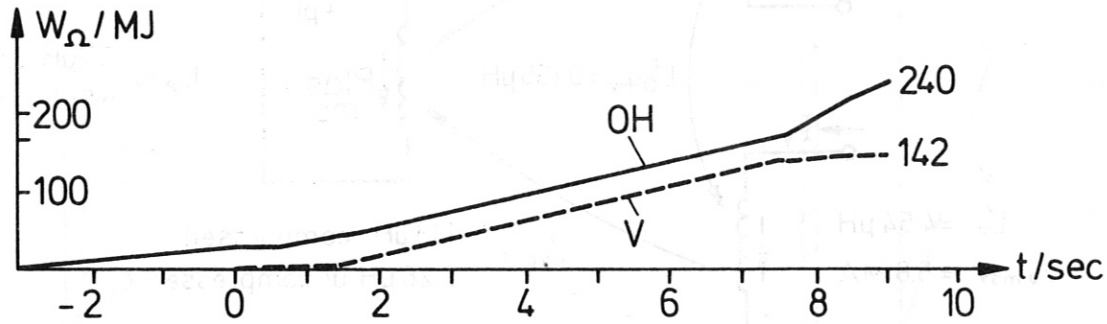

Temperature Rise centr. transf. (OH I)

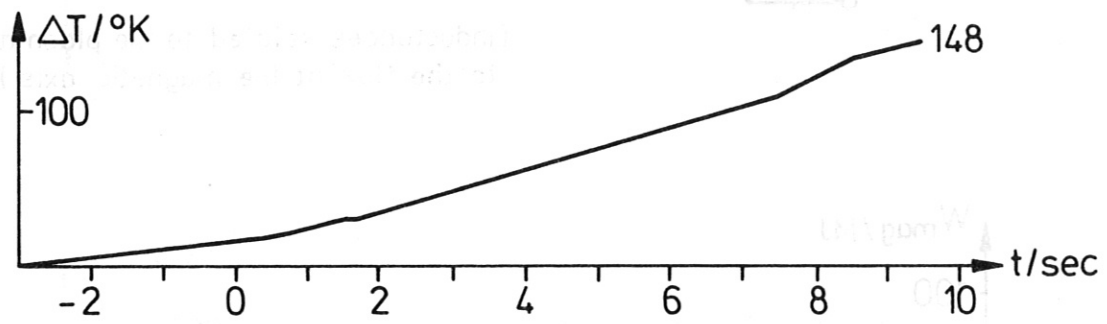

Table III

Coil	Average Current Density KA/cm^2	Steel Share %	Temp. Rise ^oK	Dissip. Energy MJ +)
OH I	8.3	25	148	169
OH II	6.5	20	67	30
OH III	6.5	0	50	19
OH IV	5.0	0	27	14
OH V	5.0	0	27	8
V I	5.0	0	36	15.5
V II	5.0	0	36	39
V III	5.0	0	36	88

assumed total filling factor for all coils: 0.85

+) total for upper and lower coils

Fig. 7: Ohmic Power, Energy and Heating

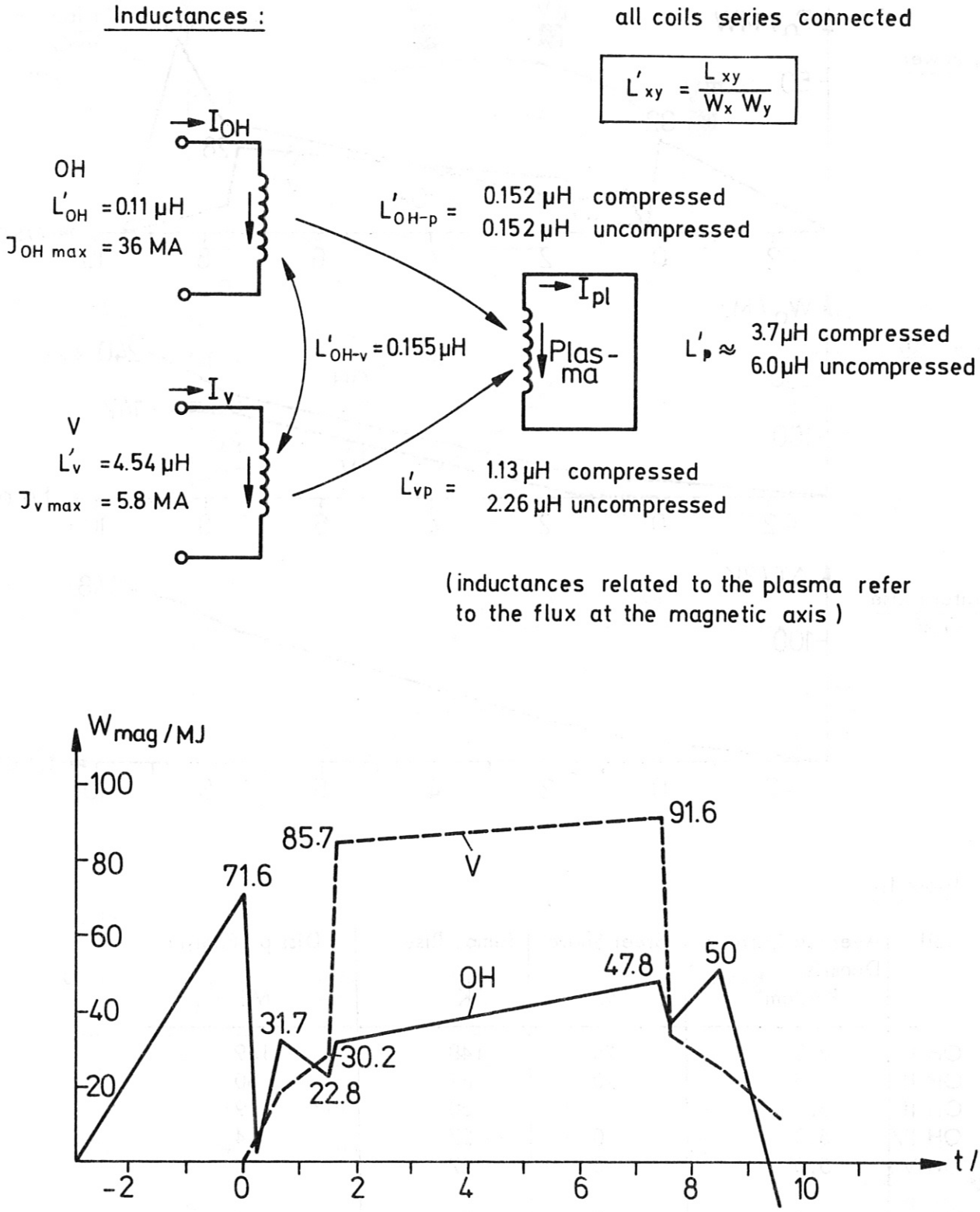

Fig. 8: Inductive Properties and Energy

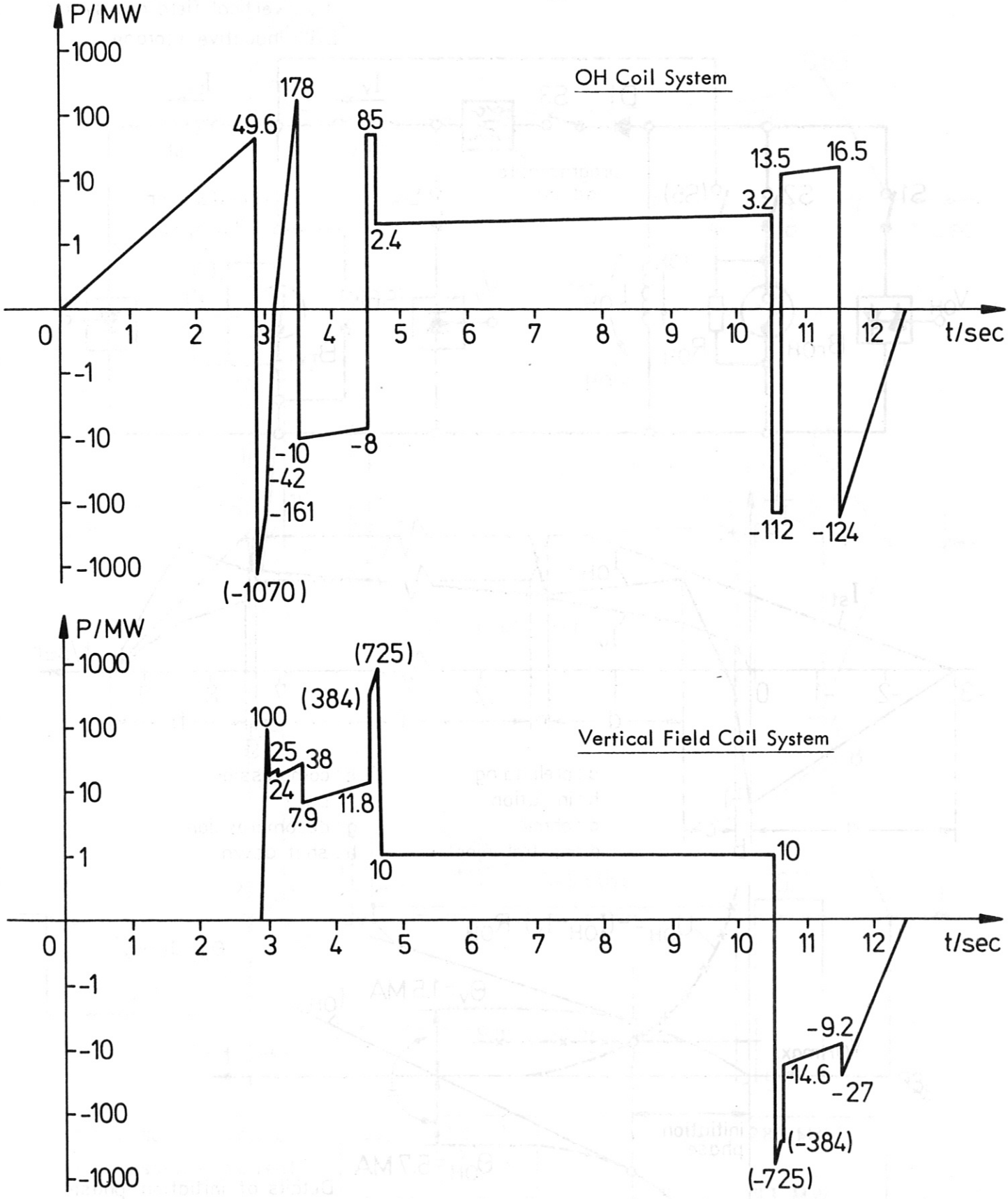

Fig. 9 : Inductive Power Requirement

L_{OH} : OH coil system
L_v : vertical-field coil system
L_{st} : inductive storage

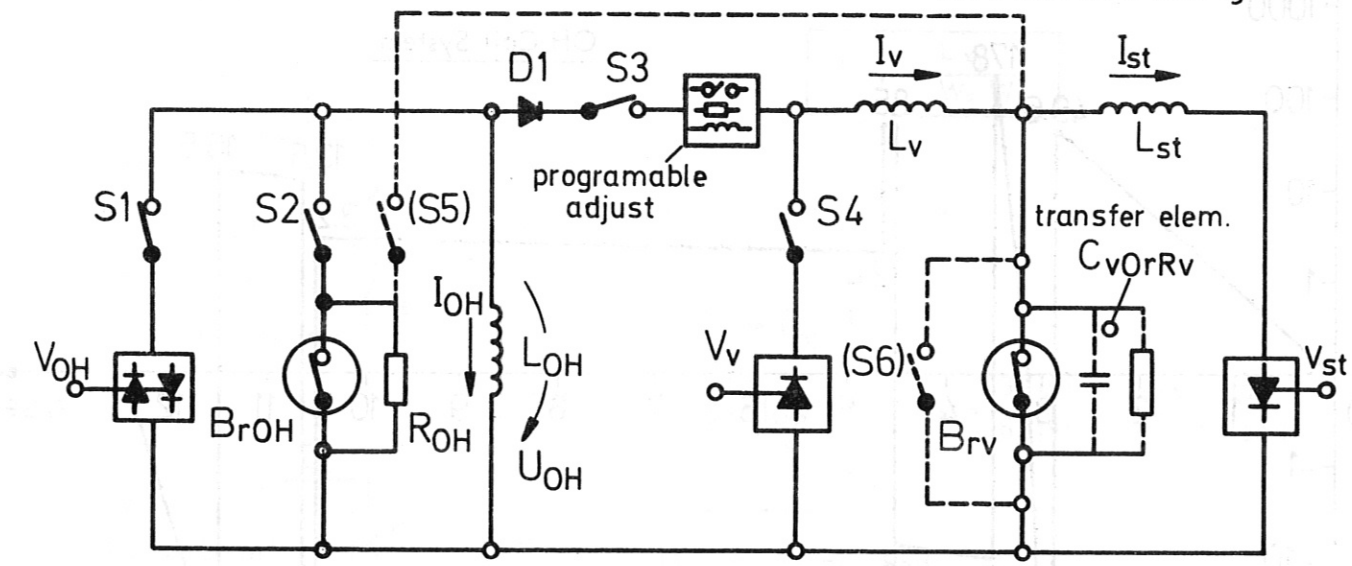

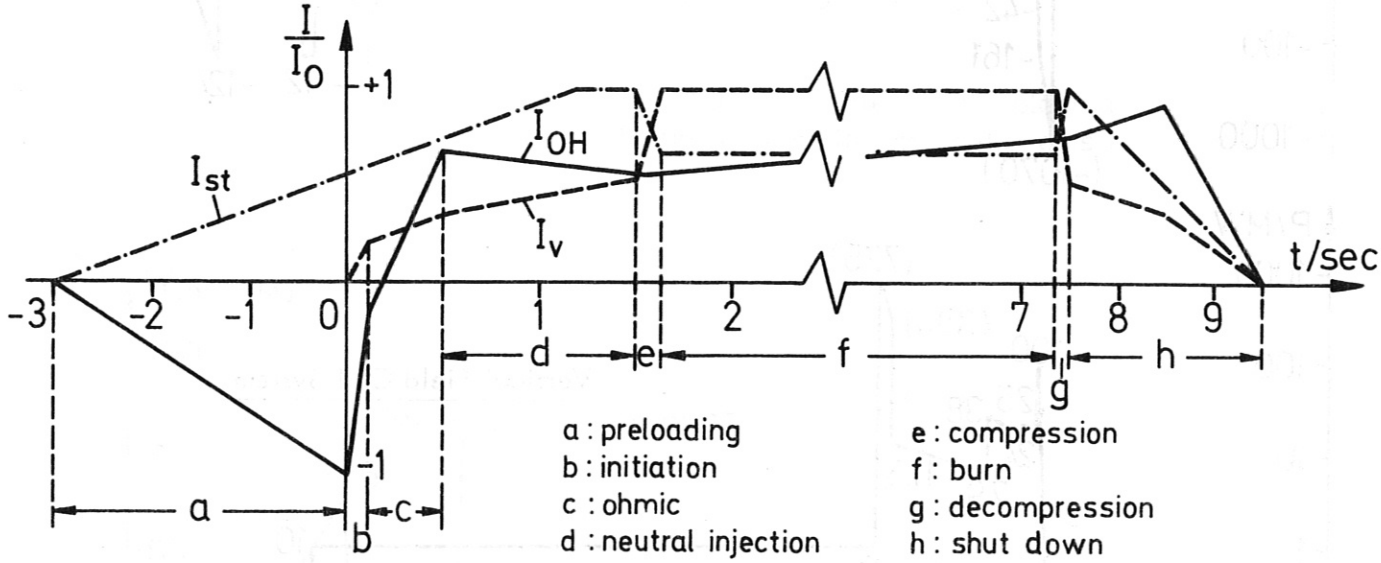

a : preloading
b : initiation
c : ohmic
d : neutral injection
e : compression
f : burn
g : decompression
h : shut down

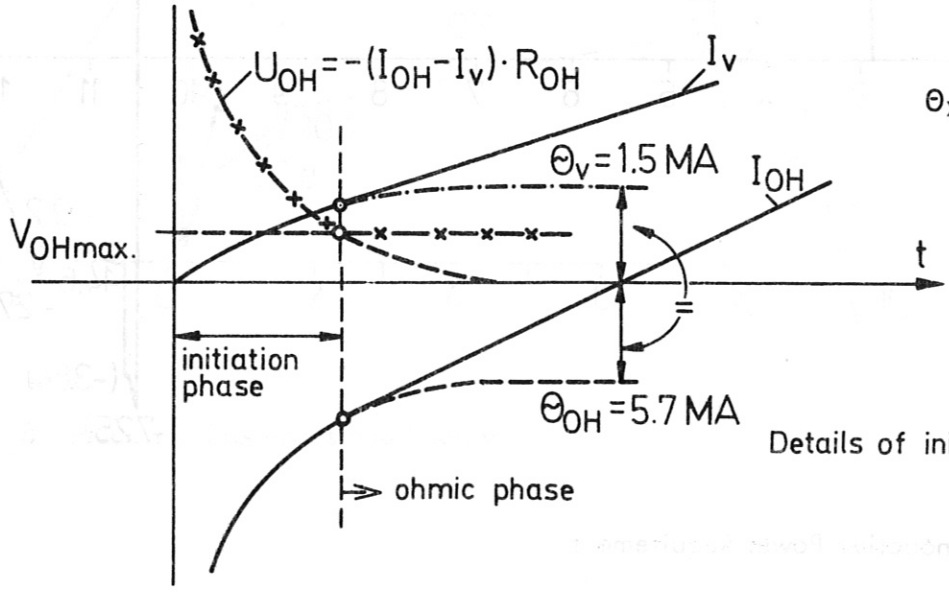

Details of initiation phase

Fig. 10: Power Supply Circuit Scheme

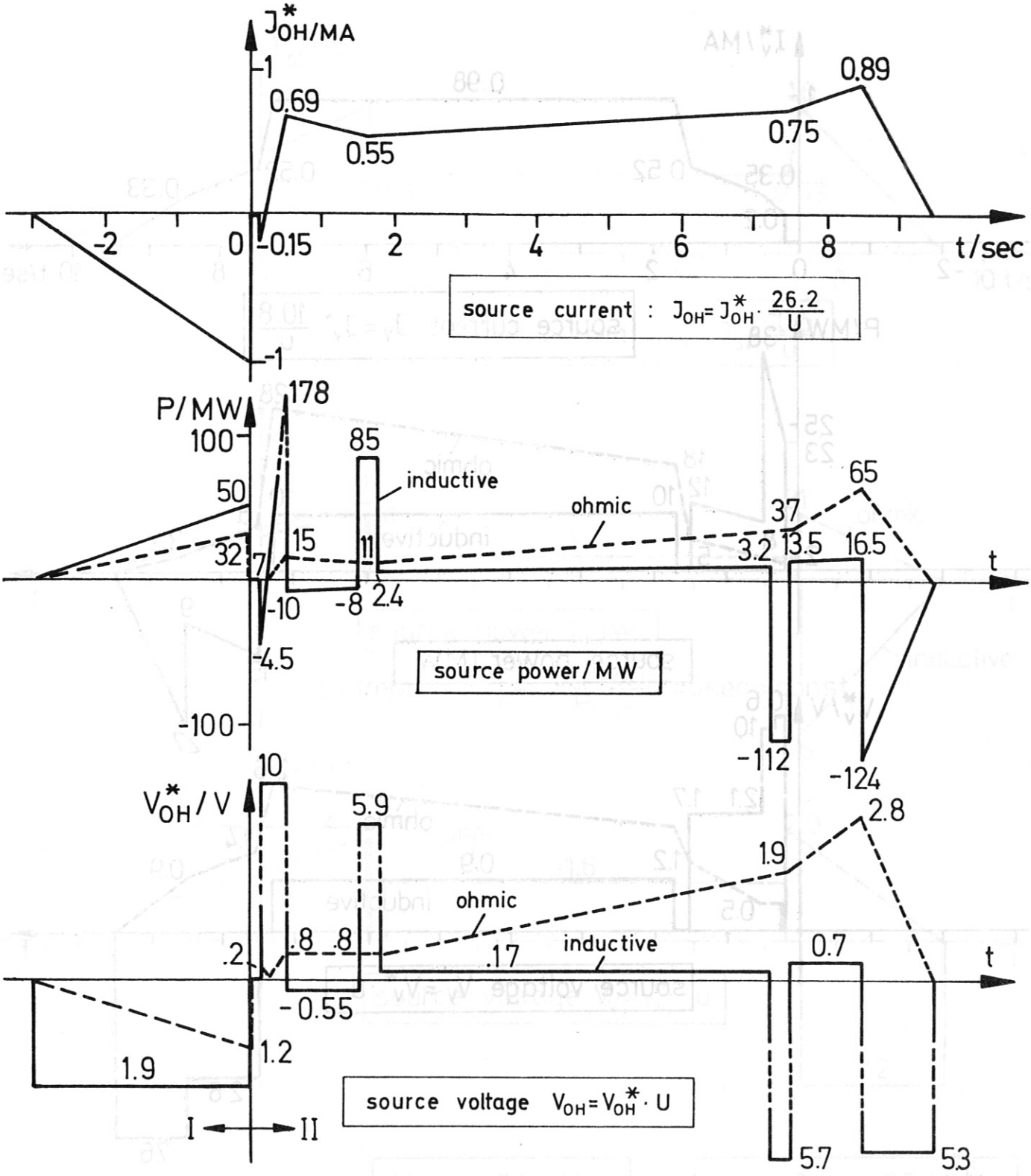

maxim. source voltage : $U_{max} = 10.8 \cdot u\,V$

maxim. source current : $J_{max} = \frac{26.2}{U}$ MA

$U_{max} \cdot J_{max} = 283$ MVA

$P_{max} = 193$ MW

$W_{tot} = 360$ MJ

total energy :

$W_{tot} = W_{magI} + W_{magII} + W_{DISS}$

$= 72\,MJ + 50\,MJ + 240\,MJ$

Fig. 11: OH-Field Source

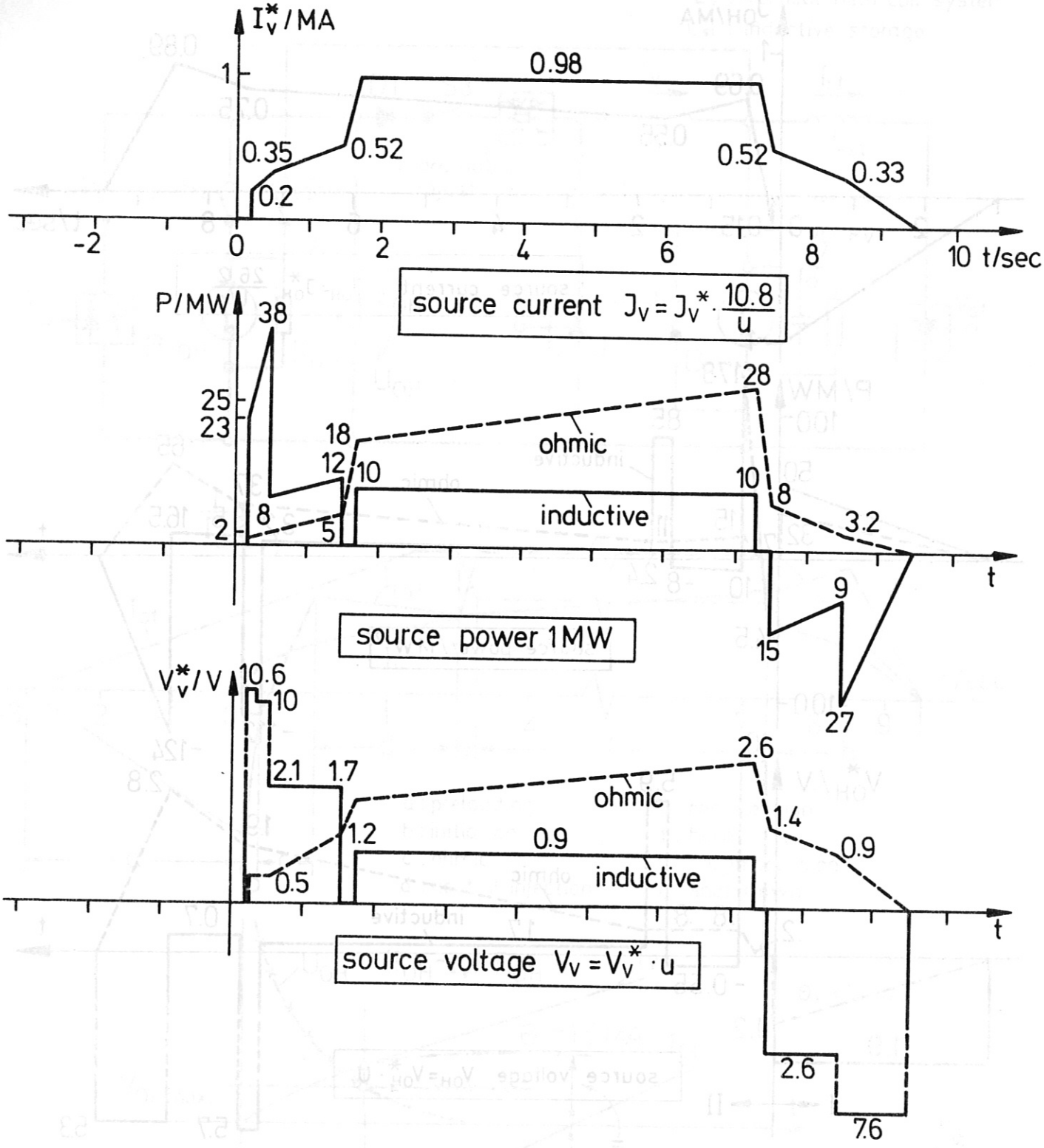

maxim. source voltage $U_{max} = 11.1\ u\,V$

maxim. source current $J_{max} = \frac{10.6}{u}\ MA$

$U_{max} \cdot J_{max} = 118\ MVA$

$P_{max} = 40\ MW$

total energy :

$W_{tot} = W_{magn} + W_{Diss} = 92\,MJ + 142\,MJ$

$W_{tot} = 234\ MJ$

Fig. 12: Vertical Field Source

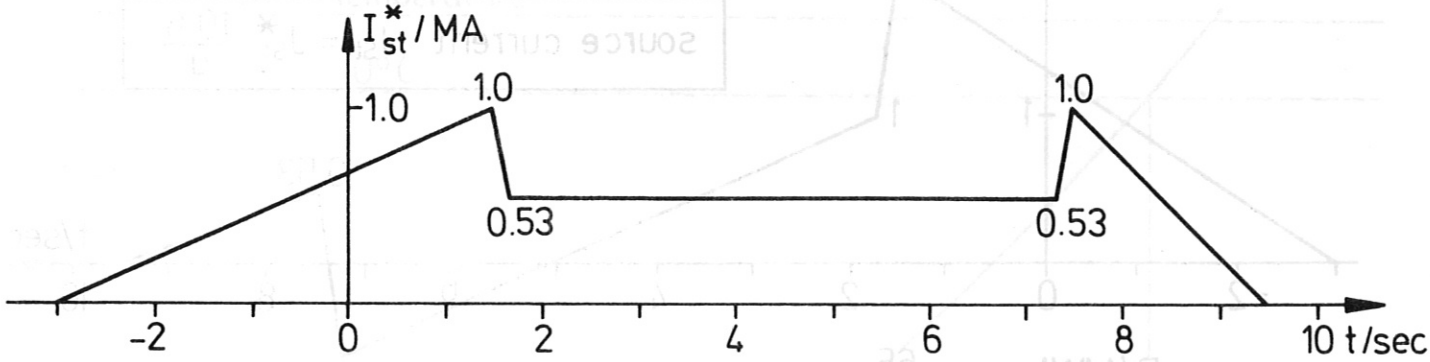

source current $J_{St} = J^*_{St} \cdot \frac{10.6}{u}$

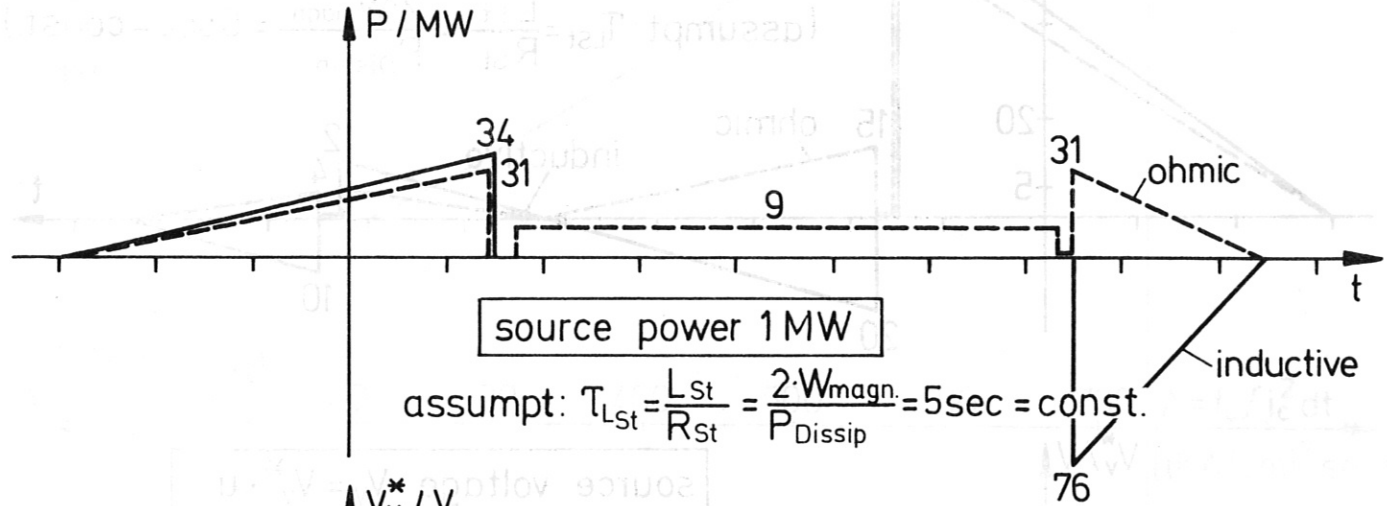

source power 1 MW

assumpt: $\tau_{L_{St}} = \frac{L_{St}}{R_{St}} = \frac{2 \cdot W_{magn.}}{P_{Dissip}} = 5\,sec = const.$

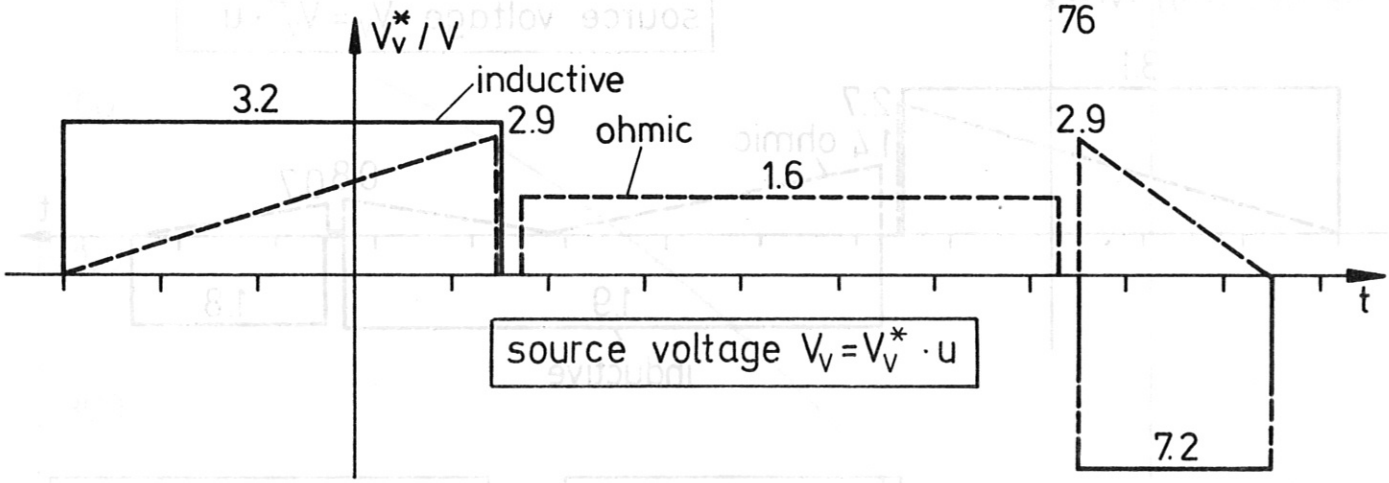

source voltage $V_V = V^*_V \cdot u$

maxim. source voltage $U_{max} = 6.1\ u\,V$

maxim. source current $J_{max} = \frac{10.6}{u}\ MA$

$U_{max} \cdot J_{max} = 65\ MVA$

$P_{max} = 65\ MW$

tot. energy

$W_{tot} = W_{magn} + W_{Dissp} = 77\ MJ + 122\ MJ$

$W_{tot} = 200\ MJ$

Fig. 13a: Storage Energy Source (capacitive transfer)

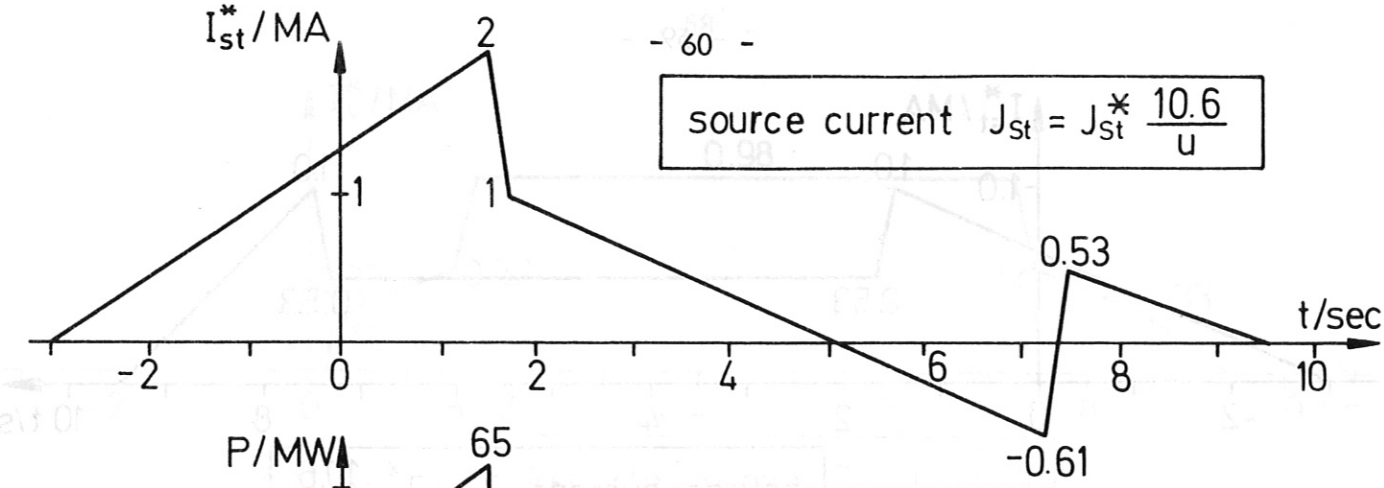

source current $J_{St} = J^*_{St} \frac{10.6}{u}$

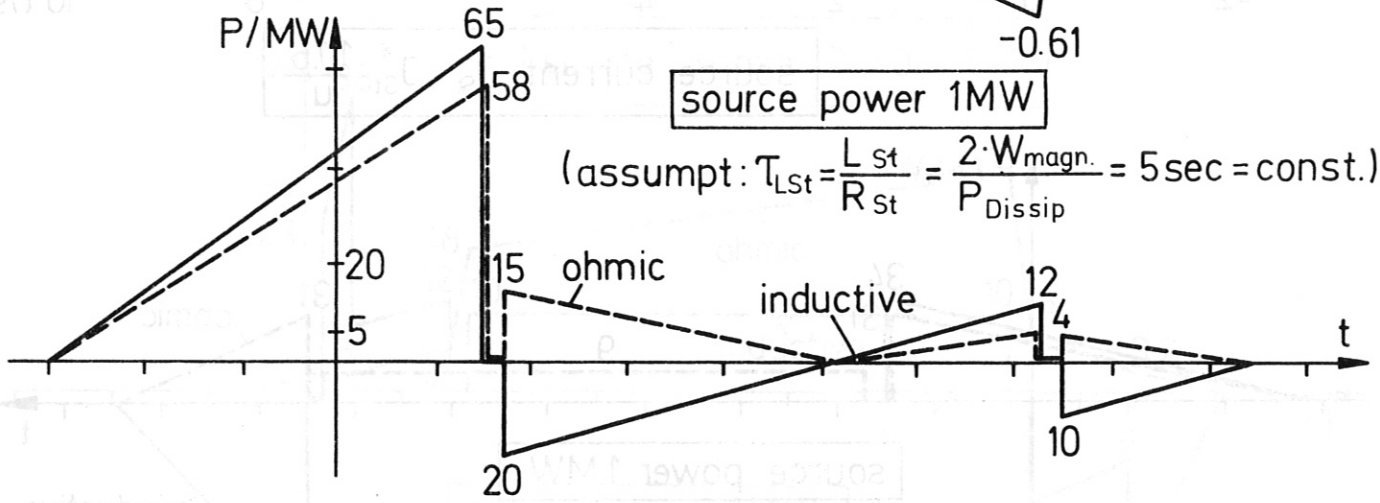

source power 1MW

(assumpt: $\tau_{LSt} = \frac{L_{St}}{R_{St}} = \frac{2 \cdot W_{magn.}}{P_{Dissip}} = 5\,sec = const.$)

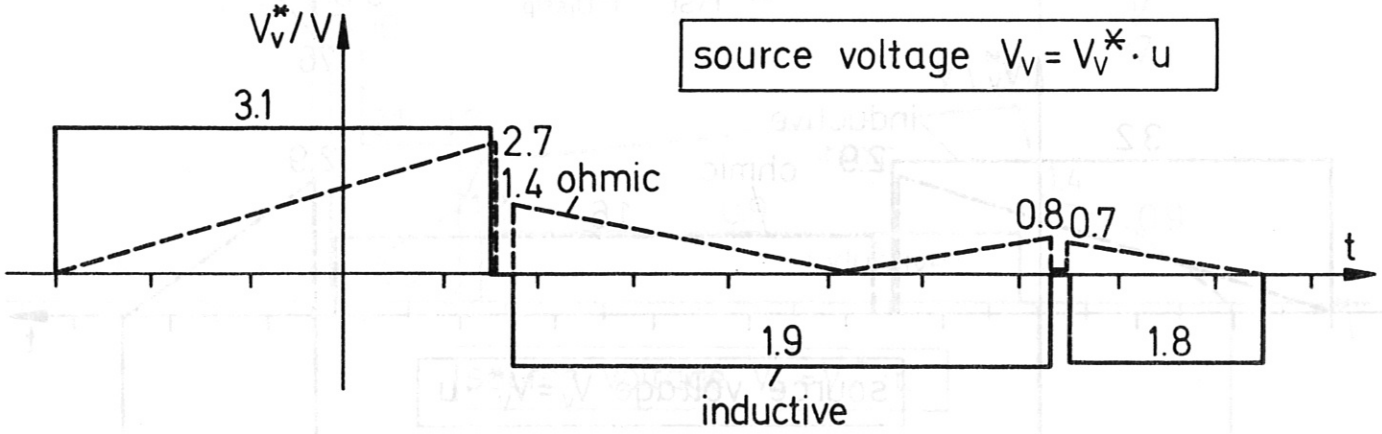

source voltage $V_V = V^*_V \cdot u$

maxim source voltage $U_{max} = 5.8\ uV$

maxim source current $J_{max} = \frac{21.2}{u}\ MA$

$U_{max} \cdot J_{max} = 123\ MVA$

$P_{max} = 123\ MW$

tot energy

$W_{tot} = W_{magn} + W_{Diss} = 144\ MJ + 112\ MJ$

$W_{tot} = 256\ MJ$

Fig. 13b: Storage Energy Source (ohmic transfer)

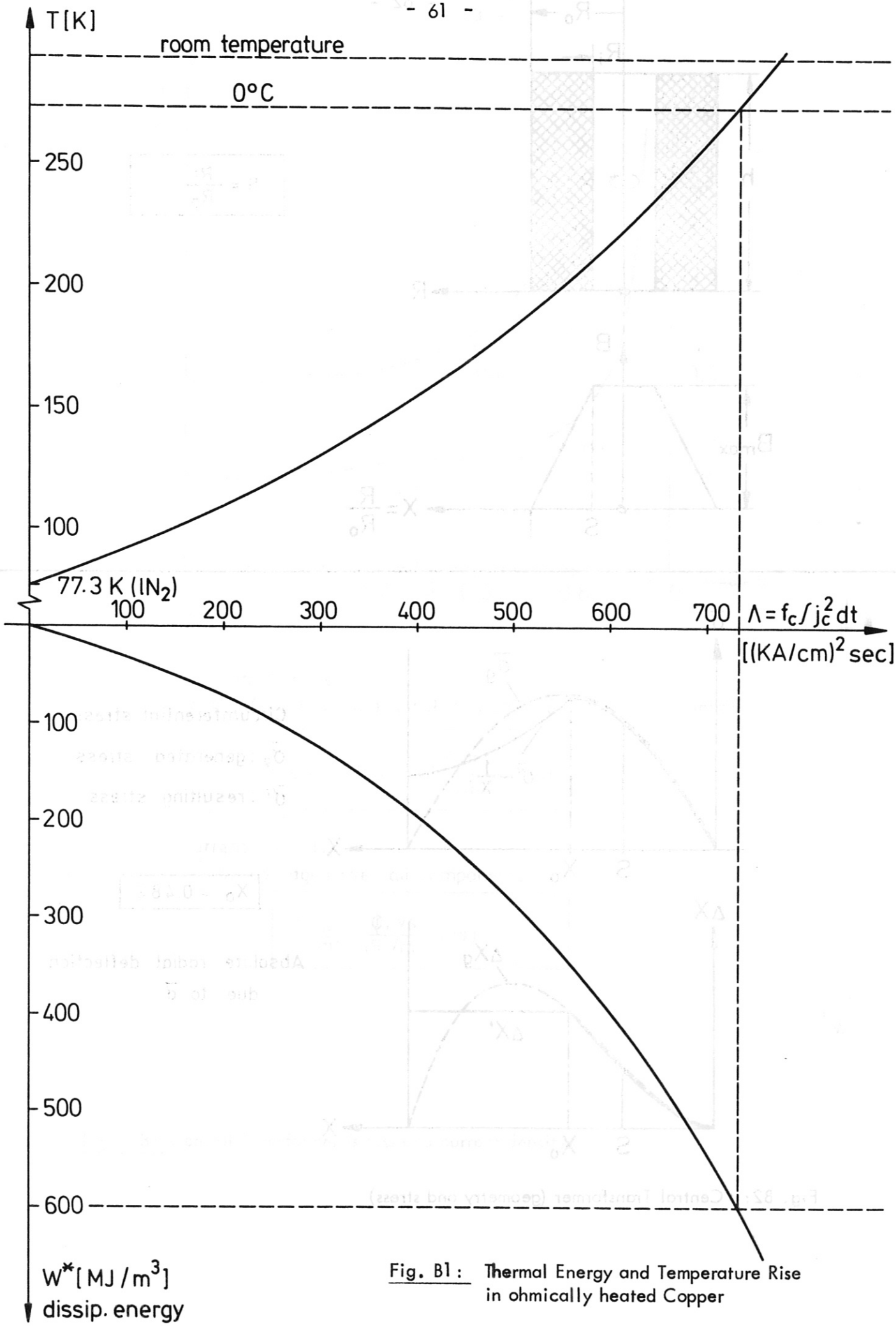

Fig. B1 : Thermal Energy and Temperature Rise in ohmically heated Copper

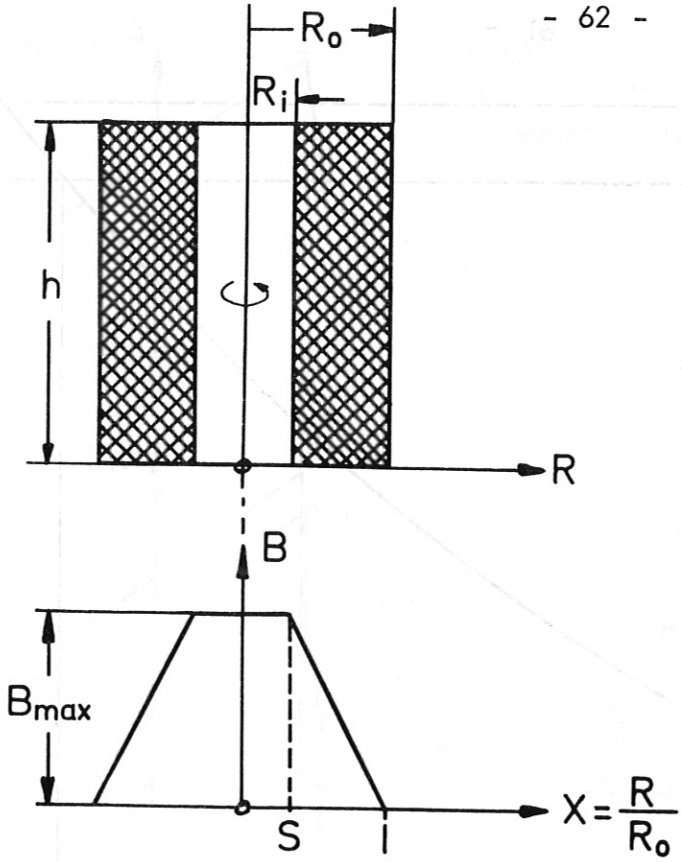

$$S = \frac{R_i}{R_o}$$

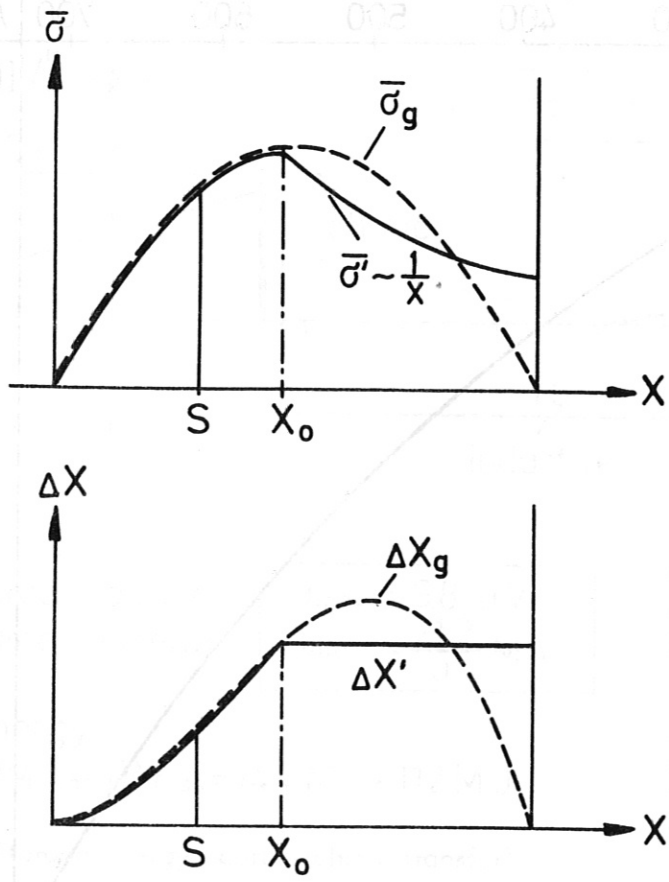

Circumferential stress

$\bar{\sigma}_g$: generated stress

$\bar{\sigma}'$: resulting stress

$$X_o = 0.482$$

Absolute radial deflection due to $\bar{\sigma}$

Fig. B2: Central Transformer (geometry and stress)

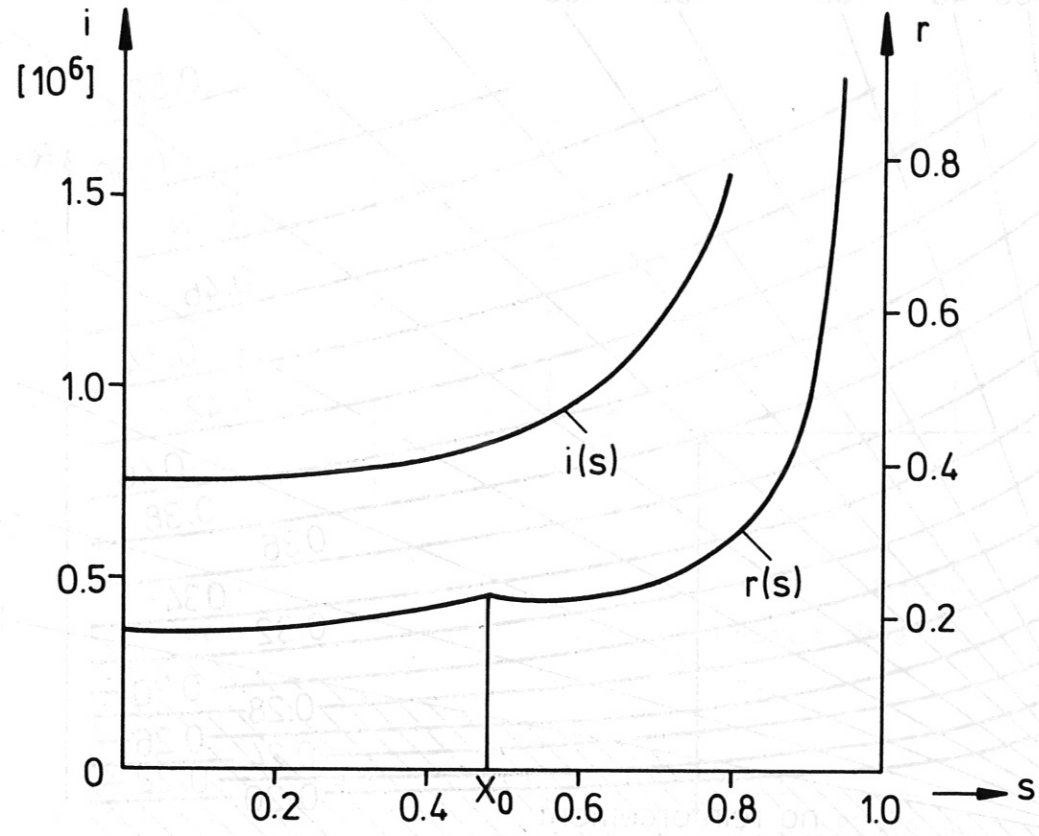

maxium stress
(circumferential and local averaged over all components)

$$\bar{\sigma}_{max}\,/\mathrm{MPa} = \frac{(\phi/vs)^2}{(R_0/m)^4}\cdot r(s)$$

current density
(local averaged over all components)

$$\bar{j}\,/\frac{A}{m^2} = \frac{\phi/vs}{(R_0/m)^3}\cdot i(s)$$

Fig. B3: Central Transformer (stress and current density)

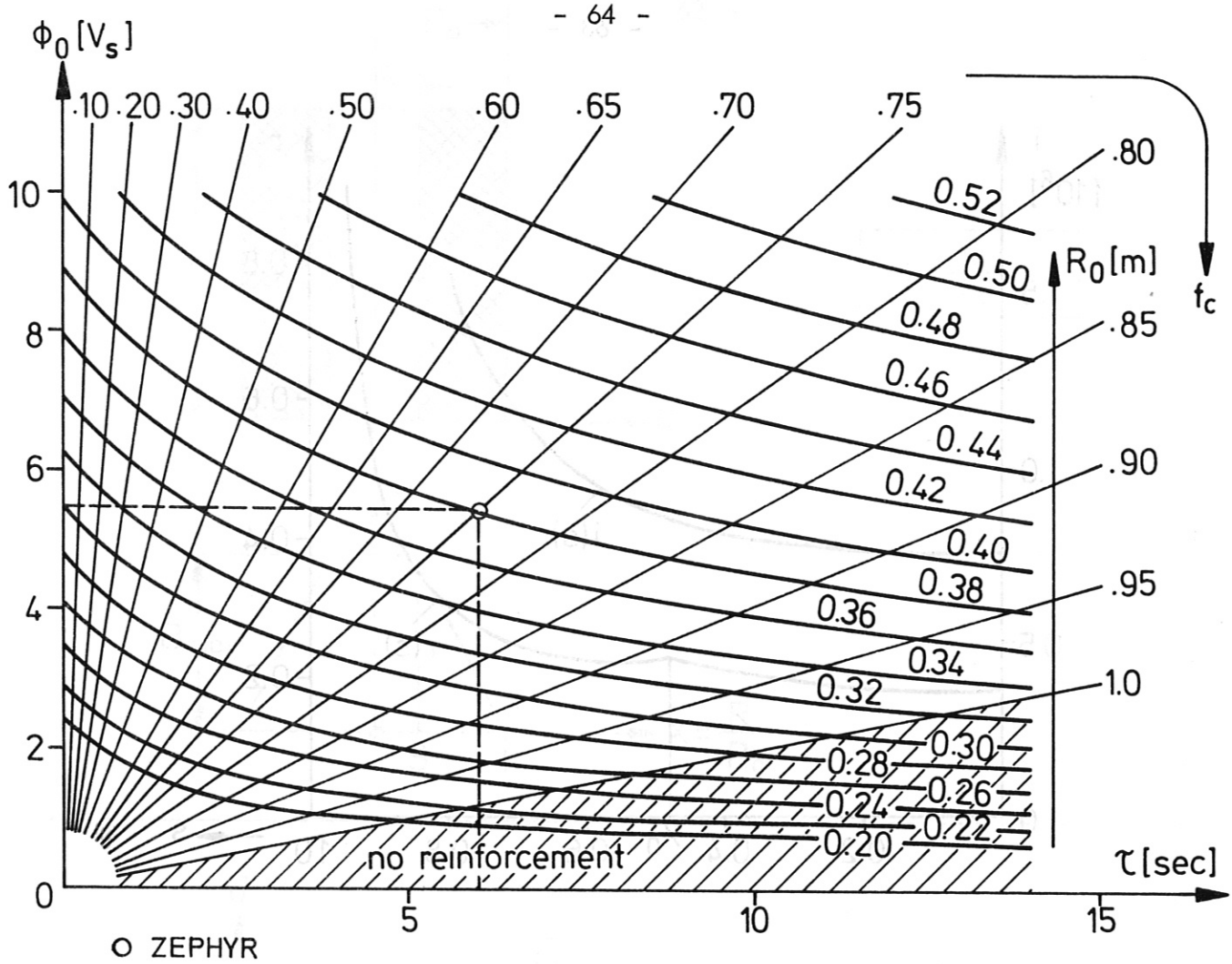

central transformer coil

material : copper reinforced by steel

$$f_c = \frac{F_{copper}}{F_{copper} + F_{steel}}$$

σ_{copper} : 150 MPa
σ_{steel} : 900 MPa

loading : $\int \phi^2 \, dt = \phi_0^2 \cdot \tau$ equivalent to

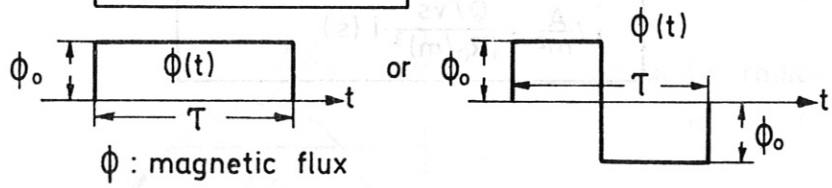

ϕ : magnetic flux

temperature rise : 77.3 K ($l.N_2$) ⟶ ≈ 280 K (adiabatic heating !)

geometry : R_o : outer radius

$$\frac{\text{inner radius}}{\text{outer radius}} = s = 0.3$$

total filling factor : $f_m = 0.8$

Fig. B4: Central Transformer

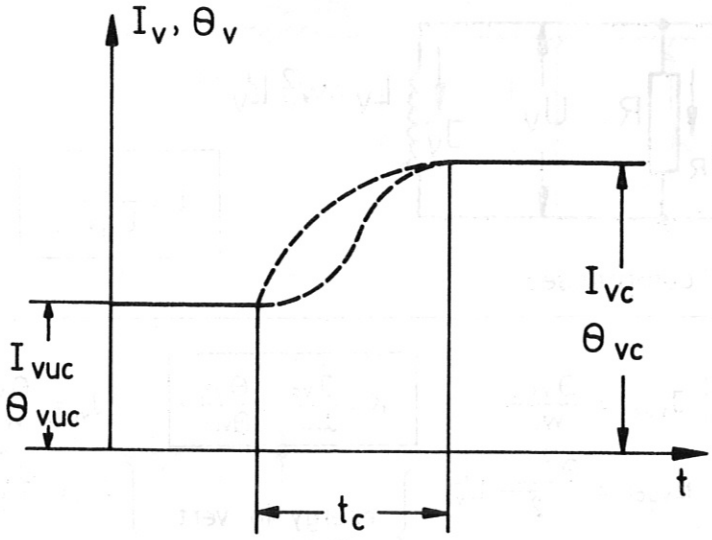

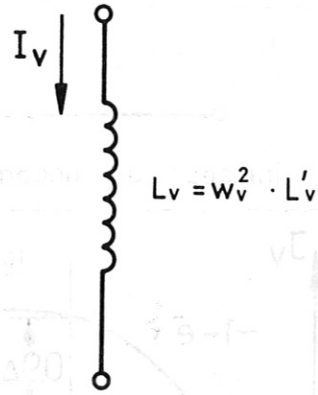

‚uc' : uncompressed
‚c' : compressed

w_v : total number of turns
t_c : compression time

coil excitement

$$\Theta_v = w_v \, J_v$$

coil current compress. ratio :

$$K = \frac{\Theta_{vc}}{\Theta_{vuc}} = \frac{J_{vc}}{J_{vuc}}$$

inductive energy :

$$E = \frac{J_v^2}{2} L_v = \frac{\Theta_v^2}{2} L'_v$$

$$\frac{E_{vc}}{E_{vuc}} = K^2$$

Θ_{vc} = 5.83 MA turns
Θ_{vuc} = 3.10 MA turns

K = 1.88

t_c = 150 msec

L_v = 4.54 µH

E_{vc} = 77.15 MJ
E_{vuc} = 21.8 MJ
ΔE_v = 55.35 MJ

Fig. C1 : Compression Circuit
Basic Requirements and Datas

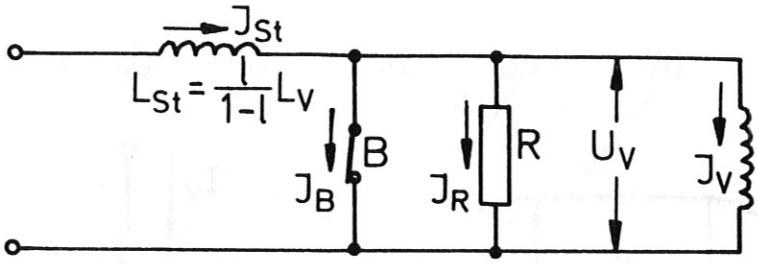

$$l = \frac{L_{st}}{L_{st} + L_v}$$

indices: ‚uc' uncompressed ‚c' compressed

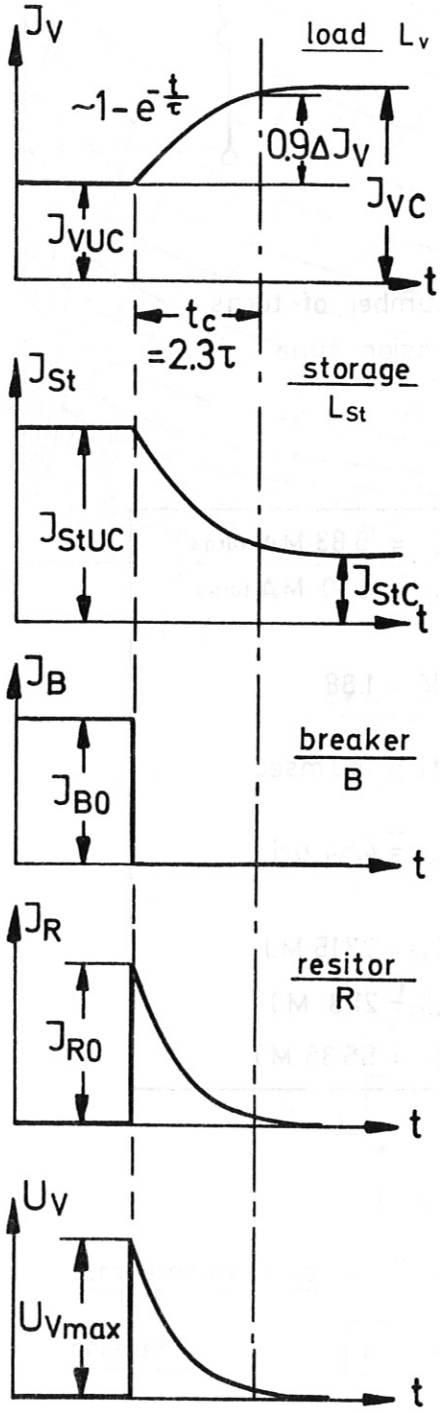

$$J_{vuc} = \frac{\Theta_{vuc}}{w_v} \qquad \boxed{K = \frac{J_{vc}}{J_{vuc}} = \frac{\Theta_{vc}}{\Theta_{vuc}}} \qquad J_{vc} = \frac{\Theta_{vc}}{w_v}$$

$$\left.\begin{aligned} E_{vuc} &= \frac{\Theta_{vuc}^2}{2} L'_v \\ E_{vuc} &= \frac{1}{K^2} E_{vc} \end{aligned}\right\} \text{ energy in vert. field coils} \qquad \left\{ E_{vc} = \frac{\Theta_{vc}^2}{2} L'_v \quad \boxed{E_{vc}} \right.$$

$$J_{Stuc} = J_{vc} \frac{l + k - 1}{K \cdot l} \qquad J_{Stc} = J_{vc}$$

stored energy:

$$E_{Stuc} = E_{vc} \frac{(l + K - 1)^2}{K^2 \, l \, (1-l)} \qquad E_{Stc} = E_{vc} \frac{l}{1-l}$$

$$E_{Stuc\,min} = E_{vc} \; 4 \left(\frac{K-1}{K}\right) \quad \text{for} \quad l = \frac{K-1}{2K-1}$$

$$J_{Bo} = J_{Stuc} - J_{vuc} = J_{vc} \frac{K-1}{2K \cdot l}$$

$$P_B = J_{Bo} \; U_{v\,max} = \frac{E_{vs}}{t_c} \cdot 4.6 \, \frac{1}{l} \left(\frac{K-1}{K}\right)^2$$

$$J_{Ro} = J_{Bo} = J_{vc} \frac{K-1}{2K \cdot l}$$

$$R = \frac{U_{v\,max}}{J_{Ro}} = \frac{2.3 \; L_v}{t_c} \cdot l$$

$$D_{Dissp} = J_{Ro}^2 \; R \cdot \frac{T}{2} = E_{vc} \frac{1}{l} \left(\frac{K-1}{K}\right)^2$$

$$U_{v\,max} = \frac{2.3}{t_c} J_{vc} \; L_v \left(\frac{K-1}{K}\right)$$

Fig. C2: Compression Circuit A

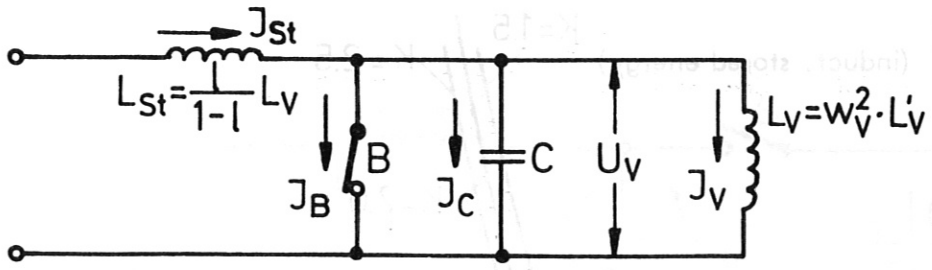

$$l = \frac{L_{St}}{L_{St}+L_V}$$

indices ‚uc' uncompressed ‚c' compressed

---

load L :

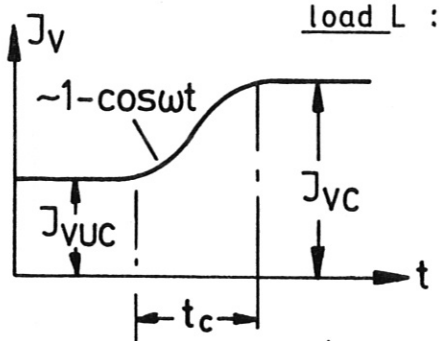

$$J_{VUC} = \frac{\Theta_{VUC}}{W_V} \qquad \boxed{K = \frac{J_{VC}}{J_{VUC}} = \frac{\Theta_{VC}}{\Theta_{VUC}}} \qquad J_{VC} = \frac{\Theta_{VC}}{W_V}$$

$$\left.\begin{aligned} E_{VUC} &= \frac{\Theta_{VUC}^2}{2} L_V' \\ E_{VUC} &= \frac{1}{K^2} E_{VC} \end{aligned}\right\} \text{energy in vert. field coils } L_V \qquad \left\{\begin{aligned} E_{VC} &= \frac{\Theta_{VC}^2}{2} L_V' \\ & E_{VC} \end{aligned}\right.$$

---

storage :

L_{St}

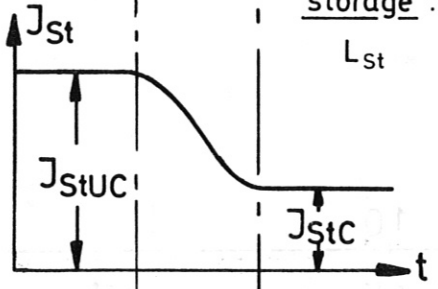

$$J_{StUC} = J_{VC}\frac{2l+(K-1)}{2Kl} \qquad J_{StC} = J_{VC}\frac{2lK-(K-1)}{2Kl}$$

stored energy :

$$\| \; E_{StUC} = E_{VC}\frac{(2l+(K-1))^2}{4K^2 l(1-l)} \;)^* \qquad E_{StC} = E_{VC}\frac{(2lK-(K-1))^2}{4K^2 l(1-l)}$$

---

breaker :

B

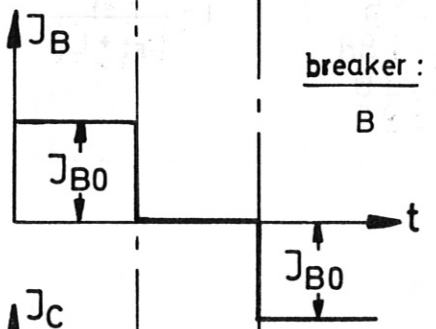

$$J_{Bo} = J_{StUC} - J_{VUC} = J_{VC}\frac{K-1}{2Kl}$$

$$\| \qquad P_B = J_{Bo} \cdot U_{Vmax} = \frac{E_{VC}}{t_c}\,\pi \cdot \frac{1}{l}\,\frac{(K-1)^2}{2K^2}$$

---

condenserbank :

C

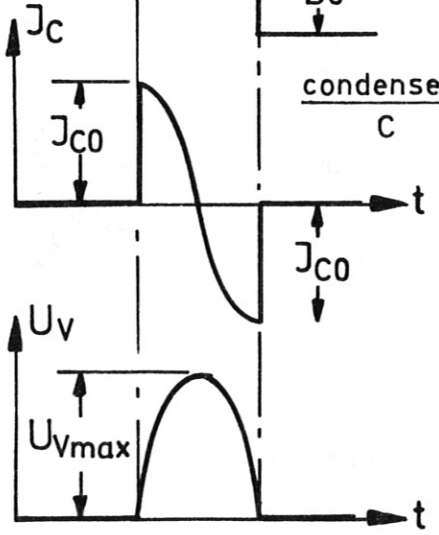

$$J_{Co} = J_{Bo} = J_{VC}\frac{K-1}{2Kl}$$

$$C = \left(\frac{t_c}{\pi}\right)^2 \cdot \frac{1}{l\,L_V}$$

$$\| \quad E_C = E_{VC}\frac{(K-1)^2}{4K^2 l} \qquad \text{storage capability)}^*$$

$$U_{Vmax} = J_{VC}\,L_V\,\frac{\pi}{t_c}\,\frac{K-1}{2K}$$

)* see fig. C 3a

Fig. C3: Compression Circuit B

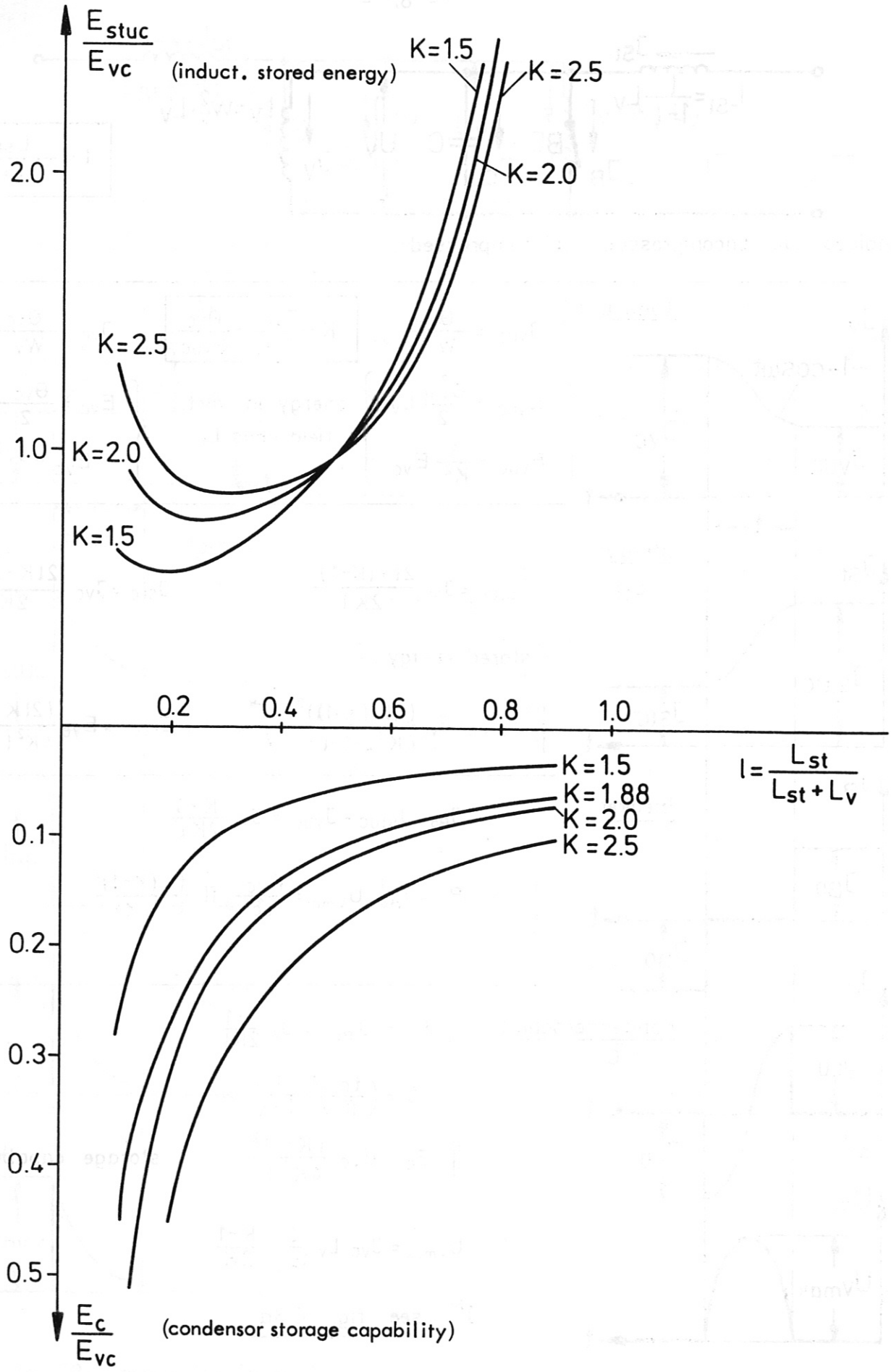

Fig. C3a: Compression Circuit B (stored energies)

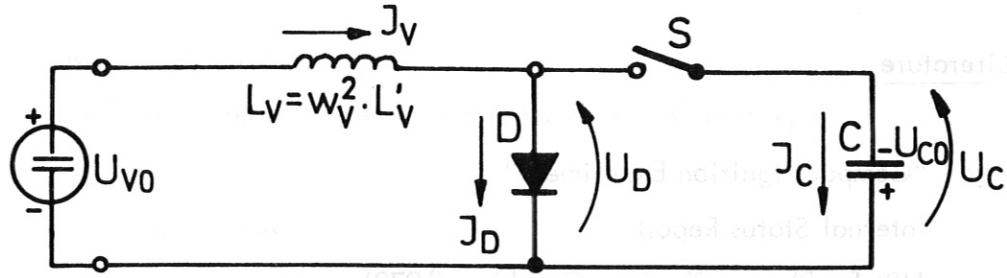

indices ‚uc' uncompressed ‚c' compressed

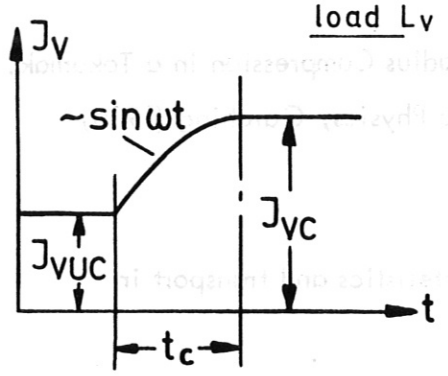

$$K = \frac{J_{vc}}{J_{vuc}} = \frac{\Theta_{vc}}{\Theta_{vuc}}$$

$$J_{vuc} = \frac{\Theta_{vuc}}{w_v} \qquad J_{vc} = \frac{\Theta_{vc}}{w_v}$$

$$\left.\begin{aligned} E &= \frac{\Theta_{vuc}^2}{2} L_v' \\ E_{vuc} &= \frac{1}{K^2} E_{vc} \end{aligned}\right\} \text{ energy in vert. field coils } L_v \qquad \left\{\begin{aligned} E &= \frac{\Theta_{vc}^2}{2} L_v' \\ E_{vc} \end{aligned}\right.$$

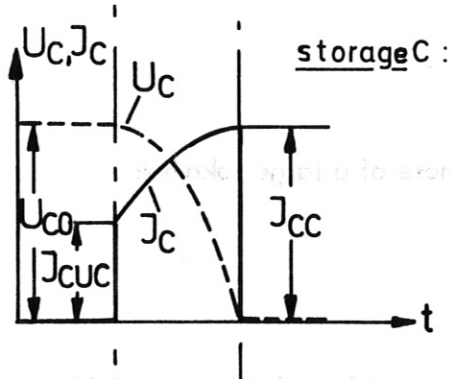

$$J_{cuc} = J_{vuc} = \frac{1}{K} J_{vc} \qquad J_{cc} = J_{vc}$$

$$C = \frac{t_c^2}{L_v} (\text{arc tg } \sqrt{K^2-1})^{-2}$$

stored energy :

$$\| \; E_c = E_{vc} - E_{vuc} = E_{vc} \left(1 - \frac{1}{K^2}\right)$$

$$\| \; U_{co} = J_{vc} \frac{L_v}{t_c} \sqrt{1 - \frac{1}{K^2}} \; \text{arc tg } \sqrt{K^2-1}$$

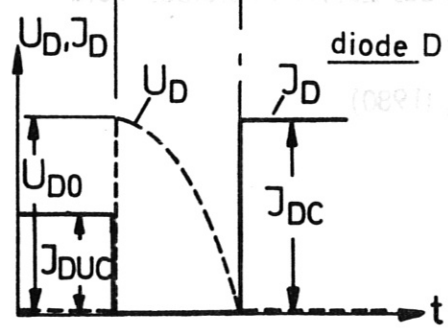

$$J_{DUC} = J_{VUC} = J_{VC} \frac{1}{K} \qquad J_{DC} = J_{VC}$$

$$U_{DO} = U_{CO}$$

$$\| \; U_{DO} \cdot J_{DC} = \frac{2 \cdot E_{VC}}{t_c} \sqrt{1 - \frac{1}{K^2}} \; \text{arc tg } \sqrt{K^2-1}$$

Fig. C4: Compression Circuit C

Literature

/1/ "Compact Ignition Experiment"
Internal Status Report
MPI for Plasma Physics, Garching (1978)

/2/ D.B. Albert, H. Winter
Adiabatic Equilibrium Calculations of Major Radius Compression in a Tokamak,
Internal ZEPHYR-Report No. 9, MPI for Plasma Physics, Garching (1980)

/3/ K. Bol et al.
"Radiation, impurity effects, instability characteristics and transport in ohmically heated plasmas in the PLT tokamak
PPPL-1492 (1978)

/4/ R.J. Hawryluk, K. Bol and D. Johnson
"Volt-second consumption during the startup phase of a large tokamak
PPPL-1508 (1979)

/5/ M. Pillsticker
"Überlegungen zum Betrieb und zur Zerstellung des ZEPHYR Poloidal-Feld-Spulen-Systems"
Internal note MPI for Plasma Physics, Garching (1980)

/6/ L. Spitzer
"Physics of Fully Ionized Gases"
Interscience Publishers, New York - London

/7/ U. Broßmann
"Theoretical Interpretation of Compound Material"
Internal note MPI for Plasma Physics Garching (1979)

/8/ F. Mast, R. Wunderlich
Personal Communication, MPI for Plasma Physics Garching

/9/ JET Proposal, EUR-JET-R5 (1975)

/10/ TFTR Proposal, PPPL 1475, PH-R-007 (1978)